Reply to reviewer 1

We would like to appreciate the valuable comments which help for improving the manuscript. In the revision, we clarify the metrics to quantitatively evaluate model performance and add some validation results concerning TC surface wind structure (Figures 5 and 6). Figures 1 and 2 are redrawn by using the result of Stage 2 only with 95% confidence levels as error bars rather than standard deviation. Careful analysis of simulated TC position revealed that some misdetection occurred for very weak TC cases. These cases are excluded from validation.
Point-to-point response are following.

That said, the goals of the manuscript are somewhat unclear.
Is the manuscript purely describing the TYMIP-G7 project framework such that it can be referenced in future studies? Or do the authors seek to describe fundamental differences in model results and attribute them to different model configurations?
The authors bounce back and forth a bit between the two and the analysis of TC forecasts (beyond mean statistics) is somewhat weak, particularly in the final quarter of the manuscript. The result that increasing resolution improves TC forecasts is not tremendously novel in the community. The analysis of the different structure of the forecasted TCs is intriguing (although require significantly more work in future manuscripts) but the authors only select a particular forecast cycle to perform analysis on, which seems tenuous (at best) given the spread in TC intensity forecasts discussed earlier in the manuscript.
My recommendation is for "major revisions." I think the authors would be well-served to tighten up the description of the simulations and model configurations, which would give a very clear citation for future papers using TYMIP-G7 data. In addition, while the authors do not need to explain why models perform differently (those are additional projects in and of themselves), it would be useful to have something more than a single forecast initialization analyzed, particularly for Figs. 6 and 8. My preference would be to present a mean structure over multiple forecast cycles and explain that these differences exist in these model configurations and require additional analysis in the future. I have elaborated on major and minor critiques below.

In this revision, we clearly state that the aim of the manuscript at the last of Section 1: describing the specification of TYMIP-G7 and a set of metrics, and showing results concerning the metrics. We deleted Figs.6 and 8 which showed simulated TC structure for a specific case, but added a composite of axisymmetric primary and secondary circulation at the mature phase of TC to discuss the difference in simulated structure of TCs. Yes, we need further works to make clear what causes

difference in simulated TC structure. Thank you for the comment.

In addition, there are phrasings that are somewhat awkward and grammatically incorrect for an English journal. I have noted some below but it is not meant to be an exhaustive list. My recommendation would be for a native English speaker to proofread this manuscript thoroughly before resubmission.

We are so sorry for our English quality. We ordered an English editing service by Enago before resubmission.

There is very little that can be said about model differences based on single forecast experiments. While I am aware that this manuscript is not intended to explain all of the physical differences (of which there might be many, particularly within the subgrid parameterization suites), I am worried that there is little utility in Fig. 6 and 8. I would anticipate being able to find cases where, for example, TCs have more asymmetric structure in GSM (even with lower resolution) or look more like observations, due to the fact that there are many forecast cycles from which to pick from. The same goes for the depth and structure of the axisymmetric circulation. Picking single members from the envelope of Fig. 4 implies that you cannot adequately understand model differences because you aren't removing run-to-run variability. In Fig. 8, it's possible that the NICAM signal (TC with lower outflow jet and shallower inflow) is a physical signal (perhaps due to the NICAM setup itself) but it also may be that that particular forecast in NICAM had more vertical wind shear than the other model configurations. My preference here would be for there to be either multiple TCs explored or perhaps some sort of average across a number of forecast cycles (say, Fig. 8 could be the average of 20 different TCs at +96 hour lead time from 20 different forecast initializations).

Thank you for the comment. It should be very useful for further detailed analyses. In the revision, we deleted Figs.6 and 8 which showed simulated TC structure for a specific case, but added a composite of axisymmetric primary and secondary circulation at the mature phase of TC.

Why is only the second stage shown in Fig. 3 but both stages are included in Fig. 4? This is especially relevant since the authors state that "track errors in MSSG were larger than those of GSM" in Stage 1, which is the opposite of the Stage 2 results (Fig. 3). If the errors associated with precipitable water (Page 8, line 25) were severe enough to eliminate their usage in Fig. 3, why weren't they eliminated in Fig. 4? Also,

why are there error bars in Fig. 4 but not in Fig. 3? Error bars should be included in Fig. 3 to give a sense as to the spread around the mean. It is difficult to understand whether those differences in track are "significant" (in either a statistical sense or just by subjectively assessing the figure).

We used the result of Stage 2 only for Figs. 3 and 4 and added error bars showing 95% confidence levels rather than one standard deviation.

The timing results are very underdeveloped. For example, what is "execution efficiency?" To be honest, I'm not sure if this adds a great deal to the manuscript. Timing studies seem most useful either a) when as many variables are constrained as possi-ble (i.e., same resolution, different physics, etc.) or b) operationally, when a wall clock time benchmark threshold is required. For example, here DFSM is much faster, so in an operational sense, a forecaster might say "why don't we just use DFSM?" However, a more rigorous timing analysis might want to demonstrate the strong and weak scaling properties of the model and what happens if different subgrid parameterizations are used. Furthermore, Table 5 currently investigates only one forecast cycle. Individual forecasts may have different timings (even with the same model) for a variety of reasons (different load on the computing cluster, how the communication is spread amongst nodes, failures/bottlenecks during I/O write to disks, etc.). My recommendation would be to just remove the table (since this is R2O) and spend a brief paragraph discussing mean timings (i.e., over multiple forecast cycles), but emphasizing that there are many, many different aspects of each model configuration that lead to the disparate timings.

Thank you for the comment. In the revision, we used computational resource for a 5-day forecast (node-hours) as a metrics to evaluate the timing of the model. The amount of resource is hardly variable among cases because computational nodes are occupied for a model experiment and disk I/O is performed from/to the work disk mounted on each computational node. We also discussed many aspects which affect timings.

The authors mention "errors" in Stage 1 forecasts multiple times during the manuscript but don't elaborate significantly. My preference would be for any changes/corrections between Stage 1 and Stage 2 that persist in the data to be noted clearly such that future analysis with TYMIP-G7 data can refer back to it (note, that if the authors corrected these issues and merely re-ran Stage 1 with the updated settings, there is no reason

to mention this as long as the "incorrect" Stage 1 data is overwritten).

We decided to rerun the experiments in Stage 1 by MSSG using this year's budget but they have not completed yet. Because Stage 2 has enough samples to examine difference in TC track, intensity, and structure, we used Stage 2 throughout the revision. Since we believe describing causes of failure in MSSG would help some model developers, we remained the description. Thank you for your understandings.

- Page 2, Line 10: '... is to avoid that transform.' Please cite a reference.
- Page 10, Line 11: '... Skamarock (2004) stated that seven times...' this is dependent on the numerical scheme and not universal across all models. See Kent et al., 2014, JCP.

Deleted.

- Page 10: Line 28: Is there anything in this manuscript that evaluates rapid intensification (RI) critically? A figure such as Fig. 5 could be useful, but if Delta_SLP (change in surface pressure) is calculated, not absolute surface pressure. Otherwise, RI seems neglected, so I wouldn't include this as a main result.

We deleted some sentences concerning RI.

- Fig. 4., it appears the initialization is too weak across all models (~5 hPa), which could propagate through the intensity forecasts at long leads. This is particularly relevant for the DFSM model which is initialized too weak yet develops TCs that are generally too strong.

Thank you for the comment. Initial bias of TC central pressure is mentioned in the revision.

Grammar/Typos:
- Page 2, Line 27: '... form on annual average in the western North Pacific...' is awkward. Could be 'Since an average of 26 TCs (XXXX) form on average in the western North Pacific....'
- Page 2, Line 39: 'to' should be 'too'
- Page 3, Line 37: '... diurnal cyclone...' should be '... diurnal cycle...'
- Page 4, Line 5: '... most activate...' should be '... most active...'
- Page 9, Line 32-33: 'However, precipitation patterns...' should be 'However, the precipitation

patters...'

All comments concerning above grammar and spelling errors are corrected in the revision. Thank you for your careful review.

Reply to reviewer 2

We would like to appreciate the valuable comments which help for improving the manuscript. In the revision, we clarify the metrics to quantitatively evaluate model performance and add some validation results concerning TC surface wind structure (Figures 5 and 6). Figures 1 and 2 are redrawn by using the result of Stage 2 only with 95% confidence levels as error bars rather than standard deviation. Careful analysis of simulated TC position revealed that some misdetection occurred for very weak TC cases. These cases are excluded from validation.
Point-to-point response are following.

This paper provides a preliminary assessment of tropical cyclone quality obtained from three high-resolution models. Although the paper is well-written, understandable and provides interesting results, I am somewhat concerned about framing the paper as a model intercomparison. Namely, I would expect a paper that lays out an intercomparison effort would provide substantive details on how one can quantify success. This is particularly evident through section 5.3, where the assessment is purely qualitative and, by avoiding any negativity about particular modeling systems, fails to call out what seem to be deficiencies in the structure of the typhoon that arises in the MSSG and DFSM models. To address this concern, it is suggested that the authors explicitly callout the metrics (computational performance, track error, intensity error, structural error) that could be used to quantitatively assess model performance, along with how one could quantify success under these metrics. This listing is analogous to section 4.1, but with further quantification of success or error under each criteria. Further, a tabulated intercomparison of the compared models that shows successes / deficiencies would be helpful to the reader to more clearly see how they intercompare.

In this revision, we clarified metrics to quantitatively evaluate model performance (Section 4.1) and the evaluation results (Section 5). Thank you for the valuable comment.

Page 6, line 6: Why is the standalone MSSG-A used when a coupled oceanatmosphere version is available?

Because the other models are not coupled with full 3D ocean model, the standalone MSSG-A was used so far. As we discussed in Section 6, we would like to examine the ocean effect using AO coupled MSSG as well as AO coupled NICAM. Thank you for the understanding.

Page 7, line 11: Does the slab ocean model react appropriately to the passing TC by

generating a cold wake?

The slab ocean model just calculates local heat budget between atmosphere and ocean slab. Therefore, no cooling due to vertical mixing or Ekman pumping, but cooling by shielding effect of short wave by clouds occurs (Page 7, lines 17-19).

Page 7, line 4-5: “split-explicit” and “horizontally explicit and vertically implicit” typically refer to different techniques. The former uses explicit sub-cycling to deal with some vertically propagating wave modes, whereas the latter uses an implicit solve for all vertical terms.

Thank you for the comment. This part has been corrected in the revision (Page 7, line 11).

Page 9, line 27: Is the appearance of the “wavy” structure of the tropical cyclone associated with Gibbs’ oscillations that arise from the spectral-transform nature in the model?

Figure 6 was deleted in the revision.

Page 9, line 35-37: Some additional discussion should be provided here regarding correctness. It seems that NICAM is the only one that produces a structure that matches observations – is that a correct assessment? Since the paper advocates for this hindcast strategy for assessing model quality, it should be more explicit on how one can actually evaluate the models using a mechanism that is not purely qualitative.
Page 10, line 7: Again, what is “correct”? The focus on qualitative model differences in this paragraph gives no insight into actually evaluations of the model.
Page 10, line 17: Again, additional information is needed on model correctness.

In this revision, we clarified metrics to quantitatively evaluate model performance (Section 4.1) and the evaluation results (Section 5). Thank you for the valuable comment.

Page 10, line 11: This is actually highly dependent on the numerical methods employed in the dynamical core and associated diffusion scheme. For a model like DFSM one would expect a finest resolved dynamical mode closer to 4dx, whereas for NICAM, which uses a co-located finite volume method, one would expect a finest resolved mode closer to 12dx. See Ullrich (2014).

Thank you for the comment. This part is deleted in the revision.

Page 11, line 13: It is stated earlier that NICAM is used in coupled atmosphere-ocean mode, so this statement is not quite correct.

The slab ocean does not calculate any ocean dynamics like vertical mixing and advection (Page 7, lines 17-19). Here, we would like to state that coupling with a 3D full ocean model is needed to examine impact of ocean cooling by TC. The statement is modified in the revision (Page 11, line 25).

Global 7-km mesh nonhydrostatic Model Intercomparison Project for improving TYphoon forecast (TYMIP-G7): Experimental design and preliminary results

Masuo Nakano[1], Akiyoshi Wada[2], Masahiro Sawada[2], Hiromasa Yoshimura[2], Ryo Onishi[1], Shintaro Kawahara[1], Wataru Sasaki[1], Tomoe Nasuno[1], Munehiko Yamaguchi[2], Takeshi Iriguchi[2], Masato Sugi[2], and Yoshiaki Takeuchi[2]

[1]Japan Agency for Marine-Earth Science and Technology, 3173-25 Showa-machi, Kanazawa-ku, Yokohama, Kanagawa 236-0001, Japan
[2]Meteorological Research Institute, Japan Meteorological Agency, 1-1 Nagamine, Tsukuba, Ibaraki 305-0052, Japan

Correspondence to: Masuo Nakano (masuo@jamstec.go.jp)

Abstract. Recent advances in high-performance computers facilitate operational numerical weather prediction by global hydrostatic atmospheric models with horizontal resolutionresolutions of ~10 km. Given further advances in such computers and the fact that the hydrostatic balance approximation becomes invalid for spatial scales <10 km, the development of global nonhydrostatic models with high accuracy is urgently needed. required.

The Global 7-km mesh nonhydrostatic Model Intercomparison Project for improving TYphoon forecast (TYMIP-G7) is designed to understand and statistically quantify the advantageadvantages of high-resolution nonhydrostatic global atmospheric models for improvement ofto improve tropical cyclone (TC) prediction. TheA total of 137 sets of 5-day simulations using three next-generation nonhydrostatic global models with horizontal resolutionresolutions of 7 km, and a conventional hydrostatic global model with a horizontal resolution of 20 km arewere run on the Earth Simulator. The three 7-km mesh nonhydrostatic models are the nonhydrostatic global spectral atmospheric Model using Double Fourier Series (DFSM), the Multi-Scale Simulator for the Geoenvironment (MSSG), and the Nonhydrostatic ICosahedral Atmospheric Model (NICAM). The 20-km mesh hydrostatic model is the operational Global Spectral Model (GSM) of the Japan Meteorological Agency.

Compared with the 20-km mesh GSM, the 7-km mesh models reduce systematic errors ofin the TC track, and intensity and wind radii predictions, but still have difficulties in predicting rapid TC intensification. The benefits of the multi-model ensemble method arewere confirmed to be valid for the 7-km mesh nonhydrostatic global models. WhereasWhile the three 7-km mesh models reproduce athe typical axisymmetric mean inner-core structure such as , including the primary and secondary circulations, the simulated TC structures and their intensityintensities in each case are very different among the models. Moreoverfor each model. In addition, the simulated track is not alwaysconsistently better than that of the 20-km mesh GSM. These results suggest that the development of more sophisticated initialization techniques and model physics is needed forto further improvement ofimprove the TC prediction.

1 Introduction

1.1 Global model

The globalGlobalA global models provideis a major tool for providing fundamental information toforfor operational weather forecasting at daily, weekly, and seasonal time scales. Moreover, such models provide furnish initial and lateral boundary conditions to limited-area models, which furnish fundamental information toforfor local-scale weather forecasts. Therefore, operational numerical weather prediction centres have been developing sophisticated global models with high resolution and accuracy. Because such models require huge computational resources, their development strongly depends on advances in high-performance computers. Recent computer progress has facilitated the reasonable operation of global

models with horizontal ~~resolution~~resolutions of ~10 km. Indeed, the European Centre for Medium-Range Weather Forecasts (ECMWF) has operated a global model with a horizontal resolution of 9 km since March 2016. Therefore, sooner or later, it is expected that all numerical weather prediction centres will operate global models with horizontal grid intervals ~~less than~~ of ≤10 km.

Developing high-resolution models with a horizontal grid spacing ~~<~~ of ≤10 km must resolve three challenges. The first is to use a nonhydrostatic equation system. In the Earth's atmosphere, hydrostatic balance is established for spatial scales ~~larger than~~ ≥10 km~~,~~ with high accuracy. Therefore, the primitive equation system, which approximates the vertical momentum equation with the hydrostatic balance equation, has been used in conventional global models. The second challenge is to use a dynamical core that effectively runs on state-of-the-art, ~~massive~~massively parallel computer systems. Many conventional global models use the spectral method in which the Legendre transform is used for the meridional expansion of certain prognostic variables. Because the computational cost of this transform increases with the third power of the number of grid points and communication costs become ~~great~~large, one ~~of the solutions~~solution is to avoid such ~~transform~~transforms~~such~~~~that transform~~ (Tomita et al., 2001). The last challenge is to implement sophisticated physical schemes suitable for high-resolution models, especially for clouds, because they can be partially resolved in ~~the~~a model with a horizontal resolution of 10 km.

書式変更: 上付き/下付き(なし)

Because developing operational numerical weather prediction models with high accuracy requires huge computational and human resources, the concept of ~~the~~ transition of research to operations (R2O) has recently been encouraged ~~recently~~. For example, the Hurricane Weather Research and Forecasting Model (Bernardet et al., 2015) and an atmosphere–ocean coupled limited-area model (Ito et al., 2015) have been developed based on R2O in the United States and Japan, respectively. In Japan, two next-generation, nonhydrostatic global atmospheric models have already been developed and used in the research community. These are called the Multi-Scale Simulator for the Geoenvironment (MSSG) and the Nonhydrostatic ICosahedral Atmospheric Model (NICAM). In addition, the Meteorological Research Institute (MRI) of the Japan Meteorological Agency (JMA) has developed a next-generation nonhydrostatic atmospheric model called the nonhydrostatic global spectral atmospheric Model using a Double Fourier Series (DFSM). To gain knowledge, to develop and improve nonhydrostatic global models and to share them with the research and operational communities are ~~one of the~~some aims of the present project ~~study~~.

1.2 TC forecasts

Tropical cyclones (TCs) are characterized by violent winds and torrential rain. These ~~causes~~events cause~~cause~~ tremendous damage to human lives, property~~,~~ and socioeconomic activity via landslides, floods~~,~~ and storm ~~surge. Since~~surges. Because ~~approximately~~ an average of 26 TCs ~~(more than~~ (≥30% of the global average) form ~~on annual average~~ in the western North Pacific ~~in a~~each year, accurate TC track and intensity ~~forecast is~~forecasts are of great concern to East Asian countries ~~for mitigating~~to mitigate the impacts of the associated disasters. The JMA has the primary responsibility for TC forecasts in the western North Pacific region as a Regional Specialized Meteorological Centre (RSMC) of the World Meteorological Organization. The ~~agency~~JMA has operated a 20-km mesh global atmospheric model ~~for predicting~~to predict weather and TC ~~track~~tracks and ~~intensity~~intensities since 2007. Therefore, upgrading their global atmospheric model is a promising approach to improve TC forecasts in the western North Pacific.

Errors in track prediction ~~of~~by the JMA operational global atmospheric model have ~~been~~ decreased on an average by half over the past 20 years (JMA, 2014~~),~~) as the operational model has been upgraded. For example, TC track prediction error in a 30-hour forecast with a 60-km mesh global model was ~200 km in 1997~~, decreasing~~ and decreased to ~100 km in 2010 with a 20-km mesh model. ~~Although~~Even though we have continuously ~~striven to~~ improved TC track prediction, ~~there are still~~ abnormally large track prediction errors called ~~"~~'forecast ~~busts"~~busts' (e.g.~~,~~ Carr and Elsberry, 2000) still ~~sometimes~~ occur. Typhoons Conson (2004) (Yamaguchi et al., 2009) and Fengshen (2008) (Yamada et al., 2016; Nasuno et al., 2016)

are typical examples. ~~Predicted tracks~~Tracks predicted by tens-of-km mesh global models for Fengshen showed serious poleward-bias recurving ~~to~~o far from the Philippine Islands~~, but~~; however, the typhoon made landfall in the Philippines according to best-track analyses (Joint Typhoon Warning Center, 2008). Yamada et al. (2016) reported that a 3.5-km mesh~~,~~ next-generation nonhydrostatic global model successfully simulated its landfall in the Philippines. ~~Increase~~Increases in the horizontal resolution of global atmospheric models with appropriate physical schemes can potentially reduce bust cases and annual mean errors of TC track ~~prediction~~predictions.

Despite the advances in TC track prediction, ~~improvement of~~improvements in TC intensity predictions by global atmospheric models ~~remains~~remain a challenge. One ~~of the factors~~factor that ~~impede~~impedes improvement ~~of~~in the intensity prediction is ~~a~~the lack of horizontal resolution to capture essential mechanisms of TC intensity ~~change~~changes. TC intensity and its variation are closely related to the inner-core structure and convective activity (e.g~~.,~~. Rogers et al., 2013; Wang and Wang, 2014). Recent studies using a high-resolution, limited-area atmospheric model show that the use of a horizontal resolution of a few kilometres is necessary to realistically reproduce the inner-core structure and associated convection (e.g. Braun and Tao, 2000; Gentry and Lackmann, 2010; Kanada and Wada, 2015). Fierro et al. (2009) examined the dependence of TC intensity prediction using horizontal resolutions from 30 km to 1 km~~,~~ and point~~point~~ed~~ing~~ out that the predicted TC intensity became~~beca~~o~~me~~become rapidly ~~-~~increasingly realistic with resolutions between 15 km and 5 km. Therefore, the use of a high-resolution global atmospheric model with a horizontal resolution ~~<~~ of <10 km is promising to improve TC intensity and track prediction.

1.3 TYMIP-G7

The ~~main~~primary objectives of the ~~"~~'Global 7-km mesh nonhydrostatic Model Intercomparison Project for improving TYphoon ~~forecast"~~forecast' (TYMIP-G7) are to understand and statistically quantify the ~~advantage~~advantages of high-resolution global atmospheric models ~~toward~~towards the improvement of TC track and intensity forecasts. The project is conducted as a strategic program of the Earth Simulator of the Japan Agency for Marine-Earth Science and Technology (JAMSTEC). We accomplish ~~the~~this objective ~~by~~via a model intercomparison of three 7-km mesh nonhydrostatic atmospheric models (DFSM, MSSG~~,~~ and NICAM) and a 20-km mesh hydrostatic operational atmospheric model of the JMA (Global Spectral Model; GSM) in various cases. Because a huge amount of data is~~are~~ produced by each model, we ~~develop~~developed an effective method to handle and visualize ~~those~~the data. Sharing the knowledge obtained in this project ~~among~~with research and operational communities ~~would~~will facilitate R2O.

In this paper, we describe the ~~specifications~~specifications of TYMIP-G7 and ~~a~~the set of metrics used to validate the model ~~performance~~performances~~performanceodel performance metrics~~. Some preliminary results concerning the metrics are also shown. This paper ~~consists of~~comprises six sections. Section 2 describes the common experimental design, including the cases and the output dataset. Section 3 briefly overviews the scientific outcomes of each model and describes the detailed specifications. Section 4 presents the metrics, analysis method~~,~~ and visualization. Preliminary results ~~on~~concerning ~~regarding~~ the advantages of high-resolution models ~~in~~for TC prediction and the simulated TC wind structure are given~~given~~presented in ~~Sect.~~Section 5. Section 6 is devoted to conclusions and future work.

2 Experimental design

We imitated JMA operational specifications to conduct 5-day numerical experiments with the models (DFSM, GSM, MSSG~~,~~ and NICAM). The JMA 6-hourly global objective analysis data were used for each model to derive atmospheric initial conditions. The data were provided based on the GSM grid system, a linear Gaussian grid with a horizontal resolution of 20 km and a hybrid sigma-pressure vertical coordinate. DFSM and GSM interpolated data directly ~~to~~onto their model grids, whereas MSSG and NICAM preliminarily interpolated the data ~~into~~onto common latitude/longitude grids and pressure

levels and then interpolated this to their model grids. A merged satellite and in situ data global daily sea surface temperature (SST) product with a horizontal resolution of 0.25° (Kurihara et al., 2006) was used for the SST oceanic initial conditions ~~of SST~~ and the sea ice concentration. Because an atmospheric model was used in the present study, SSTs for the 5-day integration ~~should be~~were given as the boundary conditions. It was assumed that an SST anomaly from an observed daily climatology on an initial date persisted during the 5-day period. ~~Although~~Even though no diurnal cycle~~cyclone~~ of SST was input ~~to~~into the models, NICAM can simulate the diurnal cycle because it is coupled with a simple bulk ocean model, as described later.

The project was implemented using the Earth Simulator, a supercomputer system operated by ~~the~~ JAMSTEC. The Earth Simulator is based on NEC SX-ACE, a distributed-memory, massively parallel vector system with a total of ~~5,120~~5120 computational nodes. Each node has one central processing unit, which ~~consists of~~comprises four processing cores~~,~~ and a 64 GB main memory. ~~Theoretical~~The theoretical peak performance of the entire system is 1.3 peta floating-point operations per second.

2.1 Cases

We conducted the project for two stages: from June 2015 to September 2015 and from October 2015 to March 2016. The first stage addressed TCs from September to October in 2013 ~~when the season was~~, during the most active~~activate~~ TC season since 1951. We ~~could calculate nine~~calculated 9 TCs in 52 runs (Table 1). However, we detected some flaws in MSSG and NICAM ~~so that~~, and we could not perform some of the numerical experiments. The second stage addressed ~~a~~the lifecycle of a TC ~~such as~~, e.g. genesis, rapid intensification, recurvature, extratropical transition in addition to the Madden–Julian ~~Oscillation~~oscillation (MJO; Madden and Julian, 1972) and ~~Boreal~~the boreal summer intraseasonal oscillation (BSISO; Wang and Rui, 1990; Wang and Xie, 1997). After we ~~improve~~improved the detected flaws, we examined 13 TCs in 85 runs (Table 2) in addition to the numerical experiments in the first stage. ~~Therefore, we analysed~~We analyse the model output obtained in the second stage ~~are analysed~~ in this paper~~papermanuscript~~.

2.2 Dataset

Model output data for every 1 or 3 hours from each experiment (Tables 1 and 2) were stored for analyses. ~~Components~~The components of the output are listed in Table 3. ~~Although~~Even though each model uses its own grid system, the output data were prepared for a regular latitude/longitude (lat/lon) grid system. In TYMIP-G7, we used GrADS file formats (~~set~~ pairs of 4-byte IEEE 754 floating-point standard with a big endian binary file~~,~~ and a control file~~s~~ in text format) that are common in the atmospheric and oceanic research fields. The domain of the output data covers the globe, including the western North Pacific Ocean (100–180° E~~,~~ 0~~°~~ –60° N). For the MJO and BSISO cases (20 runs, see Tables 1 and 2), it also covers the Tropics (30° E–100° W~~,~~ 15° S–30° N). ~~Horizontal~~The horizontal resolution of the global dataset is 1.25°. The data for the western North Pacific Ocean and the Tropics are prepared with a horizontal resolution of ~0.07° (7 km) by DFSM, MSSG and NICAM and ~0.19° (20 km) by GSM. In the vertical direction, the data were prepared on 32 common pressure levels (in hPa: 1000, 975, 950, 925, 900, 875, 850, 825, 800, 775, 750, 700, 650, 600, 550, 500, 450, 400, 350, 300, 250, 225, 200, 175, 150, 125, 100, 70, 50, 30, 20~~,~~ and 10 ~~hPa).~~).

3 Models

We ~~use~~used three 7-km mesh nonhydrostatic global atmospheric models in TYMIP-G7 (Fig. 1). The DFSM ~~has been~~was developed in the MRI of the JMA. The MSSG ~~has been~~was developed at ~~the~~ JAMSTEC. ~~The~~ NICAM ~~has been~~was developed at ~~the~~ JAMSTEC, ~~The~~the University of Tokyo~~,~~ and the RIKEN Advanced Institute for Computational Science. In addition, we ~~use the~~used GSM with a horizontal grid spacing of ~20 km to quantify the ~~advantage~~advantages of the higher-

resolution models. ~~The~~ DFSM and GSM are spectral models and MSSG and NICAM are grid models. The following ~~subsection details~~subsections detail the aforementioned models (Table 4) and the experimental design.

3.1 GSM and DFSM

~~The~~ GSM (JMA, 2013) is a hydrostatic global spectral atmospheric model using spherical harmonics. The JMA has used ~~the~~this~~it~~ model operationally to provide fundamental information for forecasts. The model was put into operation in 1988 with T63L16 resolution ~~T63L16~~ (200-km mesh), where ~~"Tx"~~'Tx' refers to ~~a~~the horizontal triangular spectral truncation with a total wavenumber x~~,~~ using a quadratic Gaussian grid~~,~~ and ~~"Ly"~~'Ly' refers to the number of vertical layers y. The resolution~~:~~~~Resolution~~ of the operational GSM increased to T106L21 (120-km mesh) in 1989, T213L30 (60-km mesh) in 1996, T213L40 in 2001, TL319L40 (60-km mesh) in 2005, TL959L60 (20-km mesh) in 2007~~,~~ and TL959L100 in 2014 (JMA, 2016), where ~~"TLx"~~'TLx' refers to ~~a~~the horizontal triangular spectral truncation with a total wavenumber x~~,~~ using a linear Gaussian grid (Hortal, 2002).

The JMA has also used ~~the~~ GSM as the principal part of an ensemble prediction system for medium-range weather forecasts. The forecast data ~~were~~are widely provided via the framework of The observing-system research and predictability experiment Interactive Grand Global Ensemble (TIGGE) for the research community. TIGGE data have been used for various applications, including TC track prediction (Yamaguchi et al., 2012, 2015) and the MJO (Matsueda and Endo, 2011). In addition, ~~the~~ GSM has been used ~~for producing~~to produce atmospheric reanalysis datasets, i.e.~~,~~ the Japanese 25-year ReAnalysis (JRA-25; Onogi et al., 2007) and the Japanese 55-year ReAnalysis (JRA-55; Kobayashi et al., 2015). MRI global climate models have been developed based on ~~the~~ GSM and have been used in climate research, such as global warming projections (e.g. Mizuta et al., 2006; Yukimoto et al., 2011) and stratospheric ~~study~~studies (e.g. Shibata et al., 1999)~~.; Mizuta et al., 2006; Yukimoto et al., 2011)~~. TC activity in ~~a~~ future ~~climate~~climates has been intensively studied using various model physics and horizontal resolutions (Murakami and Sugi, 2010; Murakami et al., 2012a, ~~b).~~ ~~21~~012b).

The MRI developed DFSM by changing the hydrostatic dynamical core of ~~the~~ GSM using spherical harmonics to a nonhydrostatic dynamical core using a double Fourier series ~~expansion~~ (Yoshimura, 2012). ~~The~~ DFSM uses the same basis functions of the double Fourier series as ~~in~~ Cheong (2000). In ~~the~~ DFSM, a fast Fourier transform is used instead of a Legendre transform in the meridional direction. Because the computational cost of the ~~Fast~~fast Fourier transform is much smaller than that of the Legendre transform, especially ~~for~~at high resolution, DFSM is applicable to finer resolution simulations. DFSM gives nearly the same results as ~~the~~ GSM using the Legendre transform; a comparison of 2-day forecasts using the 60-km resolution model was shown by Yoshimura and Matsumura (2005).

In ~~the~~ GSM and DFSM, a two-time-level, semi-implicit, semi-Lagrangian scheme (e.g.~~,~~ Hortal, 2002) is used to facilitate ~~a~~ long time ~~step~~steps for computational efficiency. The vertically conservative semi-Lagrangian scheme is used in the advection calculation (Yoshimura and Matsumura, 2003; Yoshimura and Matsumura, 2005; Yukimoto et al., 2011), and a correction method similar to that described by Priestley (1993) and Gravel and Staniforth (1994) is used for global conservation in the material transport. To save computational ~~cost~~costs, we used a reduced grid (Miyamoto, 2006) in which the number of zonal grid points is decreased, especially at high latitudes (Fig. 1).

Because the DFSM resolution is ~7 km (ML2559L100; ~~"MLx"~~'MLx' refers to a horizontal truncation with zonal wavenumber x~~,~~ using ~~spectral truncation based on~~ a linear equally-spaced latitude grid), the model applies the nonhydrostatic option, which essentially uses the same nonhydrostatic equations as used in the ALADIN-NH nonhydrostatic limited-area spectral model (Bubnová et al., 1995; Bénard et al., 2010) and the nonhydrostatic version of the Integrated Forecast System global model of ECMWF (Wedi and Smolarkiewicz, 2009). However, there are some differences in the method of integration. ~~The~~ DFSM uses a non-constant coefficient semi-implicit scheme. The preconditioned Generalized Conjugate Residual method, a fast-converging iteration method, is used to solve the simultaneous linear equations associated with~~in~~ the

semi-implicit scheme ~~of the DFSM~~ (Yoshimura, 2012). Recalculation is necessary only for the non-constant linear terms during the iteration. It is found that only a single iteration is sufficient for convergence.

Physical packages included in ~~the~~ GSM and DFSM are the same as those in the March 2014 version of the operational global atmospheric model of the JMA. A prognostic cumulus parameterization scheme (Randall and Pan, 1993) and other schemes in ~~the~~ GSM are used in ~~the~~ DFSM~~,~~ without any changes. The physical process is described in detail in the JMA (2013).

3.2 MSSG

~~The~~ MSSG is an atmosphere~~-~~–ocean coupled nonhydrostatic model aimed at a seamless simulation from global to local scales (Takahashi et al., 2006, 2013). The MSSG ~~consists of~~comprises atmospheric (MSSG-A) and ~~ocean~~oceanic (MSSG-O) components. ~~The~~ MSSG uses a conventional lat/lon grid system for regional simulations and the ~~—~~Yin~~-~~–Yang grid system (Kageyama and Sato, 2004; Baba et al., 2010), which ~~consists of~~comprises two overlapping lat/lon grids ~~that~~to avoid the polar singularity problem, for global simulations. ~~The~~ MSSG has been used in a wide range of applications. A cloud-system-resolving global ocean~~-~~–atmosphere coupled MSSG successfully simulated an observed MJO propagation (Sasaki et ~~al.~~al., 2016). A global atmosphere~~-~~–ocean coupled experiment ~~at~~with 11-km horizontal resolution with a nested region ~~of~~with 2.7-km horizontal resolution simulated sea surface cooling caused by a TC along its track (Takahashi et al., 2013). High-resolution regional atmospheric simulations have been conducted to investigate the influence of the choice of cloud microphysics scheme and in-cloud turbulence on cloud development (Onishi et al., 2011, 2012). MSSG-O with a 2-km horizontal resolution has been used to investigate the dispersion of radionuclides released from the Fukushima ~~Dai-ichi~~Daiichi nuclear power plant (Choi et al., 2013) and the effect of wind on long-term summer water temperature trends in Tokyo Bay, Japan ~~at~~, with 200-m horizontal resolution (Lu et al., 2015). MSSG-A with a 5-m spatial resolution has been used in building-resolving urban atmosphere simulations to ~~clarify~~examine the heat environments of streets (Takahashi et al., 2013).

In ~~the present~~this study, MSSG-A is ~~mainly~~primarily used. Its dynamical core is based on the nonhydrostatic equations, and it predicts the three wind components, air density~~,~~ and pressure. Each horizontal computational domain covers 4056 × 1352 grids in the Yin~~-~~–Yang lat/lon grid system. ~~Average~~The average horizontal grid spacing is 7 km. The vertical level ~~consists of~~comprises 55 vertical layers ~~at the~~with a top height of 40 km ~~with~~and the lowermost vertical layer at 75 m. The third-order Runge–Kutta scheme is used for time integration. The fast terms related to acoustic and gravity waves are calculated separately~~,~~ with a shorter time step (Wicker and Skamarock, 2002). A fifth-order upwind scheme (Wicker and Skamarock, 2002) was chosen for the momentum advection and ~~the~~a second-order weighted average flux scheme with the Superbee flux limiter (Toro, 1989) for the scalar advection. For turbulent diffusion, the Mellor–Yamada–Nakanishi–Niino level 2.5 scheme (Nakanishi and Niino, 2009) was used. The MSSG-Bulk model (Onishi and Takahashi, 2012), a six-category bulk cloud microphysics model, is used for explicit cloud physics. Model Simulation radiation TRaNsfer code version 10 (MstrnX; Sekiguchi and Nakajima, 2008) is used ~~for calculating~~to calculate longwave and shortwave radiation transfer.

During the first stage of the project, ~~an issue in which~~ extraordinary increases in precipitable water appeared in the 5-day integrations when the conventional bulk surface flux model of Zhang and Anthes (1982) was used for both land and ocean surfaces. This issue was solved by the use of the COARE 3.0 model (Fairall et al., 1996, 2003) for ocean surface fluxes~~,~~ with Zhang and Anthes (1982) being used only for land surface fluxes. This combination was used for all simulations in the second stage, and we plan to rerun ~~the~~ all the simulations in the first stage ~~are planned to be rerun~~. ~~It seems that the combination appeared to enhance MSSG prediction skill, judging from the fact that its TC track predictions were better on average than those of the GSM in the second stage, but poorer in the first stage.~~

書式変更：英語（英国）
書式変更：英語（英国）
書式変更：英語（英国）

3.3 NICAM

NICAM (Satoh et al., 2008, 2014) ~~has been~~was developed as a climate model and can explicitly resolve clouds without any convective parameterization, which is known ~~for~~to be the most ambiguous component in ~~a~~ conventional climate ~~model~~models (Randall et al., 2003). From the first appearance of realistic cloud-resolving ~~simulation~~simulations using a 3.5-km-mesh horizontal resolution by Miura et al. (2007a), NICAM has primarily been ~~mainly~~ used ~~for studying~~to study tropical meteorological systems, such as the MJO (Miura et al., 2007b, Nasuno, 2013; Miyakawa et al., 2014), TC genesis from the MJO in boreal winter (Fudeyasu et al., 2008, 2010a, 2010b), TC genesis from the BSISO in the western North Pacific (Oouchi et al., 2009; Nakano et al., 2015; Nasuno et al. 2016~~),~~) and BSISO in the northern Indian Ocean (Taniguchi et al., 2010; Yanase et al., 2010). NICAM has also been used for quasi-real-time forecast systems during field observation campaigns to support field ~~observation~~observations (Nasuno, 2013). Recent progress ~~of~~with high-performance computing ~~infrastructure~~infrastructures, such as the K-computer, a 10-petaflop supercomputer in Japan, facilitates 870-m mesh global ~~simulation~~simulations (Miyamoto et al., 2013, 2015; Kajikawa et al., 2016). This is the highest resolution to date (10 July 2016). Climate simulations (30-year) using a 14-km mesh model (Kodama et al., 2015) and large-member (10240 members) ensemble data ~~assimilation~~assimilations based on an ensemble Kalman filter (Miyoshi et al., 2015) have also been executed.

NICAM uses ~~the~~an icosahedral grid system that covers the globe with ~~almost~~a nearly uniform grid size, avoiding the polar singularity problem. Increased horizontal resolution is attained by recursively dividing horizontal grids in half. Therefore, the possible horizontal resolution is discrete and represented ~~in~~ "by the 'g-~~level,~~"level', which ~~means~~indicates the number of divisions of a horizontal grid. In this project, the 2014 version of NICAM (called NICAM.14.3) ~~is~~was used with a horizontal resolution of g-level 10, corresponding to a 7-km mesh. The vertical level ~~consists of~~comprises 38 vertical layers to a top height of 36.7 km~~,~~ with the lowest layer at 80 m. NICAM uses a fully compressible nonhydrostatic equation system for the dynamics of the atmosphere. The model uses an icosahedral grid system in the horizontal direction with the Arakawa A-grid and terrain-following coordinate with the Lorenz grid in the vertical direction. The equations are discretized using the flux form of the finite volume method ~~in flux form~~. The numerical scheme guarantees conservation of total mass and energy. The second-order Runge–Kutta scheme is primarily used for time integration, ~~but~~whereas the third-order Runge–Kutta scheme is used ~~for~~in some cases to avoid computational instability. NICAM uses the split-explicit scheme~~,~~ together~~known as~~ with the horizontal explicit and vertical implicit scheme~~,~~ to avoid the restriction of the Courant–Friedrichs–Lewy condition for acoustic waves. The NICAM Single-moment Water 6 cloud microphysics scheme (Tomita, 2008) is used for cloud microphysics without any convective parameterization. Planetary boundary layer processes are calculated using the Mellor–Yamada–Nakanishi–Niino level 2 scheme (Nakanishi and Niino, 2004~~),~~) implemented and examined by Noda et al. (2010). Longwave and shortwave radiation transfer is calculated using MstrnX (Sekiguchi and Nakajima, 2008). Land surface processes are computed by the Minimal Advanced Treatments of Surface Interaction and Runoff (MATSIRO; Takata et al., 2003). NICAM is coupled with a simple slab ocean model. This model calculates~~calculates~~variate SST based on the ~~depending on~~ local heat balance between the ocean slab and the atmosphere, and the other ~~any influence of~~ ocean dynamics, such as ~~(e.g.,~~ vertical mixing and~~,~~ advection~~,~~) are not considered. The slab has a specific heat capacity determined by its thickness (15 m). ~~of 15-m depth to simulate a diurnal cycle of SST.~~ The calculated SST is nudged with a persistent SST anomaly with an e-folding time of 7 days. ~~Surface~~The surface flux is calculated by the Louis (1979) scheme~~,~~ with sea surface roughness length parameterization by Moon et al. (2007).

During the first stage of this project, there ~~was a~~were frequent ~~problem~~problems of ~~division~~divisions by zero in MATSIRO that ~~was never~~had not been experienced in ~~the~~ simulations with coarser horizontal ~~resolution~~resolutions. This issue was fixed before simulations in the second stage, and abnormal cases in the first stage had to~~could~~ be rerun. ~~were recalculated.~~ The ~~It was confirmed that this~~ fix had a slight impact on the prediction results. During the second stage, however, two cases were ~~not~~ still ~~able~~unable to be completed ~~conducted~~ due to numerical instability (Table 2).

~~**3.4 Computer performance on the Earth Simulator**~~

~~Computational performance is one of the metrics to decide on an operational numerical weather forecast model. Table 5 summarizes computational performances of DFSM, MSSG, NICAM and GSM. Execution efficiency for each model on the Earth Simulator is 15%–17%, except for DFSM. GSM used the same model physics as DFSM, but its execution efficiency is higher than that of DFSM. This is mainly because calculation of the Legendre transform, done only in the GSM, is very substantial, but its execution efficiency is excellent. DFSM was optimized for the Earth Simulator in the project and become about four times faster than before, but there may be room for further optimization. Among the 7-km mesh models, DFSM requires the least computational resources, particularly in node-hours. This is largely because of the relatively long time step (Table 3), owing to the semi-implicit semi-Lagrangian scheme within that model. More sophisticated cloud microphysics schemes in MSSG and NICAM than that in DFSM is also a factor in increased computational cost of the first two models. MSSG requires the greatest computational resource, about twice that of NICAM, even though both models used the conventional advection schemes. The difference in node-hours between MSSG and NICAM are mainly attributable to the difference in vertical resolutions and number of vertical levels, which are sensitive to the time step setting.~~

4 Metrics, analysis~~Analysis~~ methods~~,~~ and visualization

4.1 Metrics

Here, we define the following ~~set of~~ metrics to evaluate the ~~regarding~~ TC forecast ~~by global models to validate~~ performance. ~~metrics of TC forecast by global models as follows:~~

(1) Computational~~C~~ resources for a 5-day forecast on the Earth simulator (node-hours)

(2) TC track (position) error every 6 hours of forecast time ~~along with forecast time~~ (km)

(3) TC intensity (central pressure) error every 6 hours of forecast time ~~along with forecast time~~ (hPa)

(4) Averaged radius of surface 50~~-~~-knot (25 m s^{-1}) wind (AR50) error (km)

(5) Averaged radius of surface 30~~-~~-knot (15 m s^{-1}) wind (AR30) error (km).

It is important for the operational model that the calculation is completed in less time with smaller computational resources so that we applied ~~the~~ metric (1). ~~A demand for smaller amount of computational resources is important for an operational model. This is considered by (1).~~ The metrics (2~~-~~) (5) ~~measures~~measure the accuracy of the track, intensity~~,~~ and surface wind structure prediction based on the ~~and these can be evaluated using~~ RSMC Tokyo best-track data.

4.2~~1~~ TC tracking

We extract TC ~~tracking~~ tracks ~~in each~~ from the model experiments using the hourly mean sea level pressure (SLP) data with a horizontal resolution of ~7 km for DFSM, MSSG and NICAM~~,~~ and 20 km for GSM. A TC centre is defined as a minimum SLP point from the predicted mean SLP field smoothed 100 times by a 1-2-1 filter~~,~~ for each longitude and latitude. The initial TC centre is defined within a radius of 1° from a centre position based on the RSMC Tokyo best-track data. The next centre position is defined as the minimum SLP point from the smoothed ~~mean~~ SLP field within a radius of 1° from the previous centre position. The tracking terminates when the minimum SLP points reach a ~~a proximity~~proximity of 1° from the lateral boundary in the domain of the output data. The tracking algorithm works well for ~~almost~~nearly all cases~~, but~~; however, misdetection occurred for some very weak TCs. These cases were excluded from the validation.

4.3 ~~Calculation method of~~ AR50 and AR30

The RSMC Tokyo best-track data contains ~~the~~ longest and shortest radii of 50-knot and 30~~-~~-knot wind ~~speed~~speeds and ~~its~~their direction. ~~Observed~~ AR50 and AR30 are defined as the average of the longest and shortest radii of the 50-knot and 30~~-~~-knot wind ~~speed~~speeds, respectively. The directions of the longest and shortest radii are defined by eight directions

(N, NE, E, SE, S, SW, W, and NW) in the best-track data. Therefore, we calculated the radii of the 50-kt knot and 30-kt knot wind in the model in each of the eight directions first, and then determined the direction of the longest and shortest radii. Then, the radii in those two directions arewere averaged to obtaino AR50 and AR30.

4.4342 Multi-model ensemble mean

The multi-model ensemble mean (MME) is applied to the three 7-km mesh models (DFSM, MSSG, and NICAM). MME is a simple ensemble average derived from a combination of individual models, which reduces the average forecast errorerrors relative to the best individual predictions by the individual models. MME also provides additional information onabout the forecast uncertainty, enhancing forecast confidence (Goerss, 2000; Yamaguchi et al., 2012).

4.5453 Visualization

WeTo compare the numerical experiment results among the four models visually and simultaneously, wWe have developed a Web application that allows a the display ofthe simultaneous visualizationsvisualizationmultiple s of multi-model results. simultaneously. Figure 2 shows a screen capture of this application, which portrays digital globes using Cesium.js (Analytical Graphics, Inc., 2015), a WebGL-based virtual globe and map engine. Visualization results of each model are overlaid on them. We used Volume Data Visualizer for Google Earth (VDVGE; Kawahara, 2012; Kawahara, 2015) to depict visualization results for overlayingthe overlay. VDVGE is, originally, a visualization software that exports visualization results coded in the KML format, a data format suitable for Google Earth. An option to export in the CZML format, suitable for Cesium.js, has been recently been implemented in Furthermore, we added a function to VDVGE. The for exporting visualization results in CZML, a data format suitable for Cesium.js. In tThe present Web application enables us, a user is able to view the animation display with for time-series visualization results of each model, while synchronously changing the three-dimensional viewpoint synchronously. An option to display Each each model result is displayed selectively is also implementedavailable. implementedusing buttons on top of the screen. The This application enables easy comparison of numerical experiments among the four models to be easily compared.

5 Results

5.1 Computational resources

Computational performance is one of thean important metricsmetric for forto determine decide on an an operational numerical weather forecast model. Table 5 summarizes computational performances a case at 00:00:00 UTC, 12 of DFSM, MSSG, and NICAM models consumed computational resources equivalent toand GSMwere 682, 2330, and 1155 node-hours, respectively for a case on 12 September 2013, 00:00:00 UTCComputational resources for a case at 12 September 2013, 00:00:00 UTC consumed by DFSM, MSSG, and NICAM were 682, 2330, and 1155 node-hours, respectively.; These quantities were hardly variabledid not vary greatly between cases asbecause the computational computation nodes were occupied in each calculation and the disk I/O was executed from/to the work disk mounted on each computationalecompute node.These amounts hardly fluctuate among cases because computational nodes are occupied for the each calculation and disk I/O has been done from/to a work disk mounted on each computational node. Execution efficiency for each model on the Earth Simulator is 15% 17%, except for DFSM. GSM used the same model physics as DFSM, but its execution efficiency is higher than that of DFSM. This is mainly because calculation of the Legendre transform, done only in the GSM, is very substantial, but its execution efficiency is excellent. DFSM was optimized for the Earth Simulator in the project and become about four times faster than before, but there may be room for further optimization. It should be notedNote that the computational resources required for each model are highly dependent on the model specificationspecifications of the Earth Simulator (e.g.,. the physics physicsal scheme, advection scheme, number of vertical layers, vertical resolution, and time

step) and the degree of optimization for the Earth Simulator. computational resources needed for each model are highly depend on model specification (e.g., physics schemes, advection schemes, number of vertical layers, vertical resolutions, and time steps) and degree of optimization for the earth simulator.For example, DFSM was optimized for the Earth Simulator of the project, which is about four times faster than beforethe conventional one. Among the 7-km mesh models, DFSM requires the least computational resources, particularly in node-hours. This is largely because of the relatively long time step (Table 3), owing to the semi-implicit semi-Lagrangian scheme within that model. More sophisticated cloud microphysics schemes in MSSG and NICAM than that in DFSM is also a factor in increased computational cost of the first two models. MSSG requires the greatest computational resource, about twice that of NICAM, even though both models used the conventional advection schemes. The difference in node-hours between MSSG and NICAM are mainly attributable to the difference in vertical resolutions and number of vertical levels, which are sensitive to the time step setting.

5.21 Track predictions

To quantify the advantageadvantages of the use ofusing finerhigh resolution onresolutions for TC track prediction, we examined the time series of errors of TC track prediction errors with reference to the RSMC Tokyo best track for the second stage (Figure 3). The samples used for verification are common to each model in both the first and second stages. We perform verification for each first and second stage separately because of differences in model settings (described in Sect. 2) when an atmospheric disturbance reached at least tropical depression strength.

In the first stage, TC track prediction by DFSM and NICAM showed better performance after forecast times (FTs) of 36 h and 96 h, respectively, relative to the prediction of GSM. Track errors in MSSG were larger than those of GSM. Adjustment of the surface flux scheme, which was done in the second stage to solve a precipitable water issue, may have reduced track errors in MSSG. Figure 3 addresses the time series of errors in TC track prediction in the second stage. TC track predictions by DFSM, MSSG and NICAM performed better than GSMhadhave better performance than diddoes GSM. However, the reduction in the track errors dependeddepends on the TC case. That is, the use of finer resolution alone does not always improve TC track prediction. This suggests that improvement ofimprovements in the initial conditionconditions and that of the physical processes in each model are also important required to improve track prediction.

We also validated MME using track predictions of the three models with reference to the RSMC Tokyo best-track data. MME track prediction gives gave the smallest track errors for forecast time (FT) ofFT = FT = 2484 120 hhours. The reduction rate of the MME position error from that of GSM was ~26from MME is ~24% at FT = 120 hhours relative to that of GSM. PositionThe position error of MME at that FT corresponds to that of GSM at FT = 96 h. Althoughhours. Even though MME had102 h. The relatively favourable good performance of MME appeared at medium-range time scales (FT = 84–120 h) as compared with the performance of individual model runs, consistent with the findings of Yamaguchi et al. (2012). Although MME has a promising result inresults with regard to improving TC track prediction, future work is required to achieve more robust results and to answer scientific and practical questions, such as in'in which cases is MME effective and why.?'

5.32 Intensity predictions

Figure 4 shows time series of the average central pressure and the standard deviation deviations infor each model relative to the RSMC Tokyo best-track data for the first and second stagestages. Because the global objective analysis data, which was used as initial conditions of the numerical experiments, tend to reproduce TC central pressure shallower than those in RSMC Tokyo best-track data, cases with an initial bias <20 hPa are validated. The central pressures in DFSM, MSSG and NICAM showed relatively small biasbiases compared withto the error in GSM. Thus,These results indicate that global these 7-km mesh models help decrease systematic positive errors forin the central pressure. However, the central pressure in DFSM showed over-intensification and the magnitude of the bias after FT = 54 hours becamebecomes larger

書式変更：英語（英国）

getsting biggerworth after FT = 54 h than that in GSM. BecauseAt least, the comparison between GSM and DFSM results suggests that a high-resolution model reduces systematic bias in TC intensity prediction, because both DFSM and GSM hathose models hadve the same specificationspecifications except for the horizontal resolution, this result suggests that the improvement on of suitable physics schemes suitable for such high-resolution modelmodels areis needed for accurate forecastforecasts of the central pressure.pressure TC intensity. This improvement is attributed to reduction of TC track forecast error (~100 km at FT = 120 h; Fig. 3) and better representation of TC structures, as shown in the next subsection. The GSM showed ashows gradual growth of positive bias in the central pressure byuntil FT = 84 hhours, including the initial first 24 hhours, ,whenwhereas the 7-km mesh models showed a continuous reduction in the intensity errors. of the central pressure decrease by FT = 24 h. After thethis early reduction this initial decrease, the errors of the 7-km mesh models beganbegin to grow in model-specific ways. MSSG showed aand NICAM shows gradual growth of positive bias ofin the central pressure byuntil FT = 84 hhours and then the errorerrors become saturated., NICAM keeps almostretained nearly no bias for the central pressure byuntil FT = 84 hhours and then showsshowed a slight growth of negative bias forin the negative bias for the central pressure byuntilgrowth. FT = 120 hhours. whereas DFSM had ahas gradual growth of negative bias for the central pressure byuntil FT = 120 hhours. . Noticeably, MME showed a negativeshows almost no bias for the central pressure after FT = 24 hhours. This demonstrates the advantage of MME for TC intensity and track prediction.

To evaluate characteristics of TC intensity prediction for each model, we show scatter diagrams of the relationship between predicted and RSMC Tokyo best-track central pressures (Fig. 5). First, GSM could not generally reproduce a central pressure lower than 940 hPa. DFSM sometimes reproduces a central pressure lower than 910 hPa, although such a TC frequently over-intensified after FT = 72 h. One of the reasons for such excessive intensification is the use of the same physical schemes tuned for a 20-km mesh model as that in the GSM. Through sensitivity experiments on the cumulus parameterization and cloud scheme, we confirmed that a modified physical scheme suitable to DFSM with 7-km horizontal resolution decreased the over-intensification (not shown). MSSG and NICAM reproduce a central pressure of nearly 930 hPa with relatively small standard deviation relative to the best-track data. From the standpoint of intensification rate, however, MSSG and NICAM still predicted rapid deepening of central pressure with difficulty, particularly the initiation of intensification.

5.43 Predictions of the TC wind structure

Accurate predictionpredictions of AR50 and AR30 lead to accurate estimationestimations of the area affected by TCs. Figure 5 shows the validation result of AR50 based on the RSMC Tokyo best-track data. All models had negative bias of 80–90 km even at the initial time. This negative bias is partlypartially would be caused byis partly attributed to the shallower estimation of the central pressure by about ~5 hPa (Figure 4) associated with the biases in the.), underestimation of AR50 by global objective analysis data, which was used as initial conditions of the numerical experiments. The, as well asThe difference in the interpolation methods to prepare the initial data for each model might also affect the bias. The negative biases of Aall 7-km models decreasereduced the initial negative bias at the initial time as FT went on in the early stage. The negative bias of DFSM monotonically decreases byuntildecreases by FT = 78 hours and then keptsaturates at have ~negative bias of 25 km at FT = 78– 120 hhours. The bias of MSSG decreases more rapidly byuntilreduced the bias. FT = 48 hhours and the bias turned to bebecomes positive tountil FT= = 84 hhours and then againreturns to have thea negative bias of ~20 km.kmshows error of ± 15km at FT = 48–120 h The bias of NICAM continuously decreases byuntildecreasesd FT = 66 hhours- and turned totthen becomes positive bias. At FT = 120 hhours, NICAM showed theshows a positive bias of 40 km, which hadwas a smaller magnitude than that of the initial bias. On the other handConversely, GSM showedshows little improvement ofin the negative bias so that itstheits resulting in negative bias staysremainswasstays still at ~ of 60 km at FT = 120 hhours. These results show that high-resolution models can significantly reduce the error of AR50 in which severe

書式変更：英語（英国）
書式変更：英語（英国）
書式変更：英語（英国）
書式変更：英語（英国）
書式変更：英語（英国）
書式変更：英語（英国）
書式変更：英語（英国）
書式変更：英語（英国）
書式変更：英語（英国）
書式変更：英語（英国）
書式変更：英語（英国）

impact is expected. In addition, MME has a promising result in improving the AR50 prediction: MME showed thea bias became almostof nearly zero atforbias FT = 60–120 hhours.

Figure 6 shows the validation results of AR30. All models showed theshow a the negative bias of more than 200 km at FT = 0 hhours. The negative biases of aAll 7-km models tended to decreasedecreasereduced the initial negative bias at the initial time in the early stage as FT proceeded. The negative bias of DFSM decreaseddecreasesreduced the negative bias bydecreases to 180 km byup toby FT = 36 h,hours and then relatively slowly decreaseddecreasesdecreasesreduced the bias byto 150 km byup toby FT = 120 hhours. The negative bias of MSSG shows temporally increasedtemporarily increases in the first 6 h,hourshnegative bias at FT = 0–6 h, and then decreaseddecreases.the negative bias d the negative bias The bias of NICAM continuously decreaseddecreasesreduceddecreases the negative bias up to FT = 120 hhours, resulting in thea negative bias as small asasof 35 km at FT = 120 hhours. GSM hadsve little improvement onin AR30 up to FT = 96 hours and shows thea negative bias of about ~170 km at FT = 120 hours. and little improvement can be seen These results show that high -resolution models can also reduce the error ofin AR30. However, all the models still had relatively largeer negative biases comparing with compared to the error ofin AR50. TowardTowards aTherefore Toward better prediction of TC wind structure, further improvementimprovements in the quality of theofof objective analysis and the models themselvesanalysis with the output by the modelsmodel diagnosis should beare needed. The bias of MME also decreaseddecreasesdecreasesreduced the negative bias up to FT = 120 h, buthours; however, its magnitude waisis larger than that ofinof NICAM.

AccurateAn accurate prediction of the three-dimensional TC structure canemay lead to accurate predictions of the intensity, AR30 and AR50 prediction. Because there is no high-resolution TC observation whichthat is suitable for the validation of the simulated TC structure, here we made anaa intercomparison of the compare TC wind structures simulated by the 7-km models and 20-km mesh GSM. Figure 7 shows a composite of the radius-height section of the azimuthal mean radial and tangential wind speeds structure for TCs at the time of the RSMC Tokyo best-track analysed central pressure between 920–940 hPa, corresponding, in in the lifecycle, RSMC Tokyo best-track data which ingsto the mature stage of a TC in the lifecycle. Total. A total of 347 snapshots were used for the composite analysis. If the models can perfectly simulate the TC structure perfectly, the result should be the same among thefor all models. WhereasWhile all 7-km mesh models reproduced a typical axisymmetric mean inner-core structurestructures, such as primary and secondary circulations, the simulated TC structures quite differed amongsignificantly between thediffers among 7-km models. The obviously shows diversity TCs calculated by in the DFSM had the highest maximum tangential wind speed and the smallest radius of maximum wind (RMW) amongof thethe7 km models. In addition, theits primary circulation structure was the deepest which reaches, reaching up to 100 hPa in the vertical direction and wasis the narrowest in the horizontal direction. The depth of the inflow and outflow layers in DFSM was relatively thin amongof the models withand had the strongest radial velocity. The TCs in NICAM and MSSG showed have relatively similar structure structures to each other, but; however, MSSG had thickersrelatively thickner inflow and /outflow layers. DifferenceDifferences in the heating and inertial stability in the inner-core lead to such differencedifferences in the primary and secondary circulation (Shapiro and Willoughby 1982). The differences between DFSM and these two models suggest different inner-core conditions in thermal and inertial stability (Shapiro and Willoughby 1982). Understanding the cause of differencethe differences in the simulated structures amongin the models will must lead to improvements in all the improvement of eacheachthe models.

Figure 6 shows horizontal distributions of hourly precipitation overlaid on SLP for Typhoon Wipha at 14 October 2013, 06:00:00 UTC (FT = 96 h) initiated at 10 October 2013, 06:00:00 UTC as an example. At that time, RSMC Tokyo best-track data showed that central pressure, maximum wind speed, and radius of surface wind speeds of 25 m s^{-1} (R25) were 940 hPa, 80 knot (40 m s^{-1}), and 120 nautical miles (220 km), respectively. Satellite observation (Fig. 7) suggests that convection in the inner core had an asymmetric structure and was most active in the northeastern semicircle, with spiral rain bands. GSM simulates a very weak TC (980 hPa), with maximum surface wind speed smaller than 25 m s^{-1} and a weak and

書式変更: 英語（英国）
書式変更: 英語（英国）
書式変更: 英語（英国）
書式変更: 英語（英国）
書式変更: 英語（英国）
書式変更: 英語（英国）
書式変更: 英語（英国）
書式変更: 英語（英国）
書式変更: 英語（英国）

disorganized precipitation pattern compared with those from DFSM, MSSG, and NICAM. DFSM has the most intense (897 hPa) and compact eyewall structure among the three 7-km mesh models, with R25 of ~95 km. In addition, the TC predicted by DFSM has double eyewalls. The difference of precipitation and SLP patterns between GSM and DFSM is attributed to their contrasting horizontal resolutions, because both models use the same configuration and specifications except for horizontal resolution. MSSG and NICAM simulate intensities (934 and 953 hPa, respectively) and R25 values (approximately 265 and 175 km axisymmetric means, respectively) similar to RSMC best-track analyses. However, precipitation patterns are completely different. MSSG shows a concentric eyewall, represented by a well-organized circular precipitation pattern. The horizontal scale of the eyewall is wider than that of the DFSM. NICAM predicts a band-shape precipitation pattern, indicating that the simulated TC does not establish a concentric eyewall as in DFSM and MSSG. Even though both MSSG and NICAM use explicit microphysical schemes without any cumulus parameterization, there are significant differences in the simulated TC structures.

Composite analyses of a radial-height section were done for Typhoon Wipha at the time of maximum intensity during its lifetime, using the results of 15 experiments (Table 1). Figure 8 shows radius height cross sections of azimuthal mean radial and tangential wind speeds. DFSM realistically reproduces the secondary circulation of a typical TC, represented by inflow toward the TC centre in the lower troposphere and outflow in the upper troposphere, compared with the secondary circulation of the GSM. However, the axisymmetric structure predicted by DFSM differs greatly from that by MSSG and NICAM. The simulated inflow layer in MSSG is the thickest among the three models, more than double that of DFSM. Another unique structure from MSSG is inflow just below the upper outflow layer. The TC vortex height in NICAM is shallower than that of DFSM and MSSG. For example, the maximum height of tangential wind speed = 15 m s^{-1} is ~100 hPa for DFSM and MSSG but 170 hPa for NICAM. The radius of maximum winds (RMW) in NICAM is more than twice that of DFSM. The slope of RMW simulated by NICAM is larger than that of DFSM and MSSG. Even though the horizontal resolution of the models is identical, differences in specifications such as dynamics and physical processes yields substantial differences in TC inner core structure.

Figure 9 shows the relationship between maximum axisymmetric mean tangential wind speed and RMW. X-marks show averages within bins every 5 m s^{-1}. The GSM is unable to reproduce the RMW derived from extended best-track data (mean or median RMWs are 64.6 and 55.5 km; Kimball and Mulekar, 2004), because the predicted RMW is > 100 km. Skamarock (2004) stated that seven times the horizontal grid spacing is the scale of the finest resolvable modes, which corresponds to ~140 km for GSM. Thus, it is difficult to reproduce an RMW < 100 km. The resolvable scale of the 7-km mesh model is ~50 km. MSSG and NICAM are able to reproduce the reduction in RMW with TC intensification, with a mean simulated RMW > 50 km. The reduction in RMW is consistent with observation by aircraft penetration (e.g., Fig. 12 of Stern et al., 2015). The RMW predicted by DFSM is the smallest among the four models. We need sensitivity studies to clarify which factors cause the RMW differences, which are closely related to differences in vertical structure of the inner core (Fig. 8).

6 Conclusions and future work

The TYMIP-G7 project have had beenwas implemented in two stages, from June 2015 through March 2016. The aim of the project iswas to statistically quantify and understand the advantageadvantages of high-resolution, global atmospheric models toward the improvement ofto improve 5-day TC track, and intensity and wind radii forecasts. We performed numerical experiments for manymultiple TC cases in 137 runs using three 7-km mesh global nonhydrostatic atmospheric models. These were the: DFSM, MSSG, and NICAM. We also included thea 20-km mesh global hydrostatic atmospheric model, GSM, on the Earth Simulator of JAMSTEC. We statistically evaluated errors ofin the TC track, and intensity and wind radii predictions, with the following mainprimary results.

(C1) The 7-km models statistically improve both the TC intensity and track predictions, whereas the improvement ~~of~~in the individual TC ~~track depended~~tracks depends on the case.

(C2) The MME is a promising approach to further ~~enhancement of~~enhance the TC ~~, intensity and~~ track and AR50 predictions.

~~(C3) (C3) Predicted~~The predicted~~Predicting rapid intensification is still challenging for 7-km mesh global atmospheric models.~~

~~(C4) Predicted~~ TC structure differs greatly ~~among~~between the three models~~,~~ even though they have the same horizontal resolution.

To follow up the above results ~~toward~~to further ~~improvement of~~improve TC prediction, we must answer the following questions~~: .~~

(Q1) Why are the TC predictions improved by high-resolution models?

(Q2) What causes the differences in the simulated TC structure ~~among~~in the three 7-km mesh atmospheric global models, such as the radius of the maximum winds, the eyewall slope, the inflow and outflow layers~~,~~ and the rainbands?

To answer (Q1), an intercomparison of forecasts by the 20-km mesh GSM and the 7-km mesh models (DFSM, MSSG~~,~~ and NICAM) is the first step. Concerning (Q2), the predicted TC structure depends on the physics schemes, such as cloud microphysics, planetary boundary layer~~,~~ and surface flux, as well as the dynamical core of the model. To understand the impacts of the model physics schemes, sensitivity experiments ~~are needed, e.g.,~~ altering the~~the~~~~ose~~those schemes and/or tuning parameters~~,~~ will be ~~needed~~required.~~.~~

In addition, the following topics are suggested for future work:

(F1) Extended-range forecasts, contributing to TC genesis and MJO/BSISO forecasts;

(F2) Atmosphere~~-~~ ocean coupled experiments to examine impacts on TC intensity and track and MJO/BSISO;

(F3) Further high-resolution experiments to study impacts of better inner-core representation on TC ~~intensity~~intensities and ~~track~~tracks; and

(F4) Data assimilation to contribute ~~to model validation~~ for validating the models and understanding ~~of~~the TC processes and model ~~initialization~~initializations.

These topics are addressed below.

An advantage of global models for TC prediction over limited-area models is the coverage of ~~multiscale~~multi-scale atmospheric phenomena~~,~~ from a mesoscale vortex to synoptic environments. Because TC genesis strongly depends on synoptic environments modulated by the MJO/BSISO, global models should be used for its forecasting. Indeed, Nakano et al. (2015) and Xiang et al. (2015) showed that TC genesis is predictable up to ~~2~~two weeks in advance; this great skill in TC genesis forecasting was attributed to its strong ~~skill in~~ ability to forecast BSISO/MJO ~~forecasting~~. We are conducting extended-range (longer than ~~2~~two weeks) forecast experiments using the four models in several cases~~,~~ and will investigate the advantage of high-resolution modes.

In the present project, atmosphere models ~~have been~~were used ~~thus far~~, except for NICAM, which is coupled with a simple slab ocean model. However, studies have shown that fully coupled atmosphere~~-~~ ocean ~~-coupled~~ processes are essential for especially slow-moving, intense TCs (Yablonsky and Genis, 2009).~~.~~ These processes affect the TC structure and ~~thereby~~therefore the track and intensity. In addition, a~~an~~a fully coupled atmosphere~~-~~ ocean ~~-coupled~~ model is ~~more skilful~~better for MJO/BSISO forecasts. MSSG is already capable of coupling MSSG-A with MSSG-O (Sasaki et al., 2016; Takahashi et al., 2013). ~~Also~~In addition, NICAM has been coupled with the Center for Climate System Research Ocean COmponent Model (COCO; Hasumi, 2006). Therefore, we will use these coupled global models to examine the impacts of global atmosphere~~-~~ ocean processes on TC forecasts.

To improve the high-resolution models, the validation of simulated phenomena using observations is essential. ~~Understanding~~An understanding of the essential processes and the modelling ~~thus require~~therefore requires high-resolution

spatiotemporal ~~observation~~observations. Recent advances in satellite observations furnish quantitatively and qualitatively rich observational data. However, the spatiotemporal resolution is still insufficient for the validation of TC ~~structure~~structures simulated by high-resolution models. Aggressively developing data assimilation techniques using satellite observations (e.g~~.~~. Zhang et al., 2016, Okamoto et al., 2016) is a promising means of obtaining high-resolution, spatiotemporal, three-dimensional TC ~~structure~~structures, including at the cloud convection scale (~O(1 km)). In addition, applying such cloud-resolving ~~analysis~~analyses to deriving the initial conditions of high-resolution models may improve TC prediction.

Data availability

The ~~ initital~~initial and boundary data for the models and model outputs are available under a collaborative framework between MRI, JAMSTEC~~,~~ and related ~~institute~~institutes or ~~university~~universities.

Acknowledgements

This project was conducted as ~~"~~'The Earth Simulator Strategic Project with Special ~~Support"~~Support' of JAMSTEC. All numerical experiments were run on the Earth Simulator (NEC SX-ACE). ~~The~~This study was partly supported by HPCI Strategic Programs for Innovative Research (SPIRE) Field 3, the FLAGSHIP 2020 project of the Ministry of Education, Culture, Sports, Science and Technology (MEXT~~),~~) and KAKENHI 26282111, 26400475~~,~~ and 15K05292 of the Japan Society for the Promotion of Science (JSPS). The authors thank Ms~~.~~ Mikiko Ikeda, Mr~~.~~ Yuichi Saitoh~~,~~ and Mr~~.~~ Hiromitsu Fuchigami for supporting the experiments on the Earth Simulator. The authors also acknowledge Mr~~.~~ Hideaki Kawai and Mr~~.~~ Eiki Shindo for the fruitful discussions. The schematic diagram of the NICAM grid was provided by Professor Masaki Satoh.

References

Analytical Graphics, Inc.: Cesium, http://cesiumjs.org, (accessed 8 Jul. 2016), 2015.

Arakawa, T., Yoshimura, H., Saito, F., and Ogochi, K.: Data exchange algorithm and software design of KAKUSHIN coupler Jcup, Procedia Comput. Sci., 4, 1516–1525, 2011.

Baba, Y., Takahashi, K., Sugimura, T., and Goto, K.: Dynamical core of an atmospheric general circulation model on a yin–yang grid. Mon. Wea. Rev., 138, 3988–4005, 2010.

Bénard, P., Vivoda, J., Mašek, J., Smolíková, P., Yessad, K., Smith, Ch., Brožková, R. and Geleyn, J.-F.: Dynamical kernel of the Aladin-NH spectral limited-area model: Revised formulation and sensitivity experiments. Quart. J. Roy. Meteor. Soc., 136, 155-169, 2010.

Bernardet, L., Tallapragada, V., Bao, S., Trahan, S., Kwon, Y., Liu, Q., Tong, M., Biswas, M., Brown, T., Stark, D., Carson, L., Yablonsky, R., Uhlhorn, E., Gopalakrishnan, S., Zhang, X., Marchok, T., Kuo, B., and Gall, R.: Community Support and Transition of Research to Operations for the Hurricane Weather Research and Forecasting Model, Bull. Amer. Meteor. Soc., 96, 953-960, doi: 10.1175/BAMS-D-13-00093.1, 2015.

Braun, S. A., and Tao, W.-K.: Sensitivity of high-resolution simulations of Hurricane Bob (1991) to planetary boundary layer parameterizations, Mon. Wea. Rev., 128, 3941–3961, 2000.

Bubnová, R., Hello, G., Bénard, P., and Geleyn, J.-F.: Integration of the fully elastic equations cast in the hydrostatic pressure terrain-following coordinate in the framework of the ARPEGE/Aladin NWP system. Mon. Wea. Rev., 123, 515-535, 1995.

Carr III, L. E., and Elsberry, R. L.: Dynamical tropical cyclone track forecast errors. Part I: Tropical region error sources. Wea. Forecast., 15, 641-661, doi: 10.1175/1520-0434(2000)015<0641:DTCTFE>2.0.CO;2, 2000.

Cheong, H.-B.: Application of double Fourier series to the shallow-water equations on a sphere. J. Comput. Phy., 165, 261-287, 2000.

Choi, Y., Kida, S. and Takahashi, K., The impact of oceanic circulation and phase transfer on the dispersion of radionuclides released from the Fukushima Dai-ichi Nuclear Power Plant, Biogeosci., 10, 4911-4925, doi:10.5194/bg-10-4911-2013, 2013.

Fairall, C.W., Bradley, E.F., Rogers, D.P., Edson, J.B., and Young, G.S., Bulk parameterization of air-sea fluxes for Tropical Ocean-Global Atmosphere Coupled-Ocean Atmosphere Response Experiment, J. Geophys. Res., 101, 747-3764, 1996.

Fairall, C. W., Bradley, E. F., Hare, J.E., Grachev, A. A. and Edson, J. B.: Bulk Parameterization of Air-Sea Fluxes: Updates and Verification for the COARE Algorithm, J. Clim., 16, 571-591, 2003.

Fierro, A. O., Rogers, R. F., Marks, F. D., and Nolan, D. S.: The Impact of Horizontal Grid Spacing on the Microphysical and Kinematic Structures of Strong Tropical Cyclones Simulated with the WRF-ARW Model, Mon. Wea. Rev. 137, 3717-3743, doi: 10.1175/2009MWR2946.1, 2009

Fudeyasu, H., Wang, Y., Satoh, M., Nasuno, T., Miura, H., and Yanase, W.: Global cloud-system-resolving model NICAM successfully simulated the lifecycles of two real tropical cyclones, Geophys. Res. Lett., 35, doi: 10.1029/2008GL036003, 2008.

Fudeyasu, H., Wang, Y., Satoh, M., Nasuno, T., Miura, H., and Yanase, W.: Multiscale Interactions in the Life Cycle of a Tropical Cyclone Simulated in a Global Cloud-System-Resolving Model. Part I: Large-Scale and Storm-Scale Evolutions. Mon. Wea. Rev., 138, 4285-4304, doi: 10.1175/2010MWR3474.1, 2010a.

Fudeyasu, H., Wang, Y., Satoh, M., Nasuno, T., Miura, H., and Yanase, W.: Multiscale Interactions in the Life Cycle of a Tropical Cyclone Simulated in a Global Cloud-System-Resolving Model. Part II: System-Scale and Mesoscale Processes*. Mon. Wea. Rev., 138, 4305-4327, doi: 10.1175/2010MWR3475.1, 2010b.

Gentry, M. S., and Lackmann, G. M.: Sensitivity of simulated tropical cyclone structure and intensity to horizontal resolution, Mon. Wea. Rev., 138, 688–704, doi: 10.1175/2009MWR2976.1, 2010.

Goerss, J. S.: Tropical Cyclone Track Forecasts Using an Ensemble of Dynamical Models. Mon. Wea. Rev., 128, 1187–1193, doi:10.1175/1520-0493(2000)128<1187:TCTFUA>2.0.CO;2., 2000.

Gravel, S. and Staniforth, A.: A mass-conserving semi-Lagraingian scheme for the shallow-water equations. Mon. Wea. Rev., 122, 243-248, 1994.

Hasumi, H.: CCSR Ocean Component Model (COCO) version 4.0. CCSR Rep 25. The University of Tokyo, Chiba, Japan, 2006.

Hortal, M.: The development and testing of a new two-time-level semi-Lagrangian scheme (SETTLS) in the ECMWF forecast model. Q. J. R. Meteor. Soc., 128, 1671-1687, doi: 10.1002/qj.200212858314, 2002.

Ito, K., Kuroda, T., Saito, K. and Wada, A.: Forecasting a Large Number of Tropical Cyclone Intensities around Japan Using a High-Resolution Atmosphere–Ocean Coupled Model, Wea. and Forecast., 30, 793-808, doi: 10.1175/WAF-D-14-00034.1, 2015.

Japan Meteorological Agency: Outline of the operational numerical weather prediction at the Japan Meteorological Agency. Appendix to WMO technical progress report on the global data-processing and forecasting system and numerical weather prediction,188p.http://www.jma.go.jp/jma/jma-eng/jma-center/nwp/outline2013-nwp/index.htm, 2013.

Japan Meteorological Agency: Annual Report on the Activities of the RSMC Tokyo -Typhoon Center, 90p, http://www.jma.go.jp/jma/jma-eng/jma-center/rsmc-hp-pub-eg/AnnualReport/2014/Text/Text2014.pdf, 2014.

Japan Meteorological Agency: The Upgrade History of the Global Spectral Model. http://www.wis-jma.go.jp/ddb/latest_modelupgrade.txt, 2016.

Joint Typhoon Warning Center: 2008 Annual Tropical Cyclone Report, 116p, http://www.usno.navy.mil/NOOC/nmfc-ph/RSS/jtwc/atcr/2008atcr.pdf

Kageyama, A. and Sato, T.: The Yin-Yang Grid: An Overset Grid in Spherical Geometry. Geochem. Geophys.Geosyst., 5, Q09005, doi:10.1029/2004GC000734, 2004.

Kajikawa, Y., Miyamoto, Y., Yoshida, R., Yamaura, T., Yashiro, H. and Tomita, H.: Resolution dependence of deep convections in a global simulation from over 10-kilometer to sub-kilometer grid spacing, Prog. Earth Planet. Sci., 3, 16, doi:10.1186/s40645-016-0094-5, 2016

Kanada, S. and Wada, A.: Numerical study on the extremely rapid intensification of an intense tropical cyclone, Typhoon Ida (1958). J. Atmos. Sci., 72, 4194–4217. doi: 10.2151/jmsj.2015-037, 2015.

Kawahara, S., Onishi, R., Goto, K. and Takahashi, K., Realistic Representation of Clouds in Google Earth, Proc. SIGGRAPH Asia 2015 VHPC, Doi: 10.1145/2818517.2818541, 2015.

Kawahara, S.: VDVGE, http://www.jamstec.go.jp/ceist/aeird/avcrg/vdvge.en.html, (accessed 27 April. 2016), 2012.

Kimball, S. K., and Mulekar, M. S.: A 15-year climatology of North Atlantic tropical cyclones. Part I: Size parameters. J. Clim., 17, 3555–3575, 2004.

Kobayashi, S., Ota, Y., Harada, Y., Ebita, A., Moriya, M., Onoda, H., Onogi, K, Kamahori, H., Kobayashi, C., Endo, H., Miyaoka, K. and Takahashi, K.: The JRA-55 Reanalysis: General Specifications and Basic Characteristics, J. Meteor. Soc. Jpn., 93, 5-48, doi: 10.2151/jmsj.2015-001, 2015

Kodama, C., Yamada, Y., Noda, A. T., Kikuchi, K., Kajikawa, Y., Nasuno, T., Tomita, T., Yamaura, T., Takahashi, T. G., Hara, M., Kawatani, Y., Satoh, M. and Sugi, M.: A 20-year climatology of a NICAM AMIP-type simulation. J. Meteor. Soc. Japan, 93, 393-424, doi:10.2151/jmsj.2015-024, 2015.

Kurihara, Y., Sakurai, T. and Kuragano, T.: Global daily sea surface temperature analysis using data from satellite microwave radiometer, satellite infrared radiometer and in-situ observations (in Japanese), Weather Bull., 73, s1–s18, 2006.

Louis, J. F.: A parametric model of vertical eddy fluxes in the atmosphere, Bound.-Layer Meteor., 2, 187-202, 1979.

Louis, J. F., Tiedtke, M., and Geleyn, J. F.: A short history of the operational PBL parameterization at ECMWF. Proc. Workshop on Planetary Boundary Layer Parameterization, Reading, United Kingdom, ECMWF, 59–79, 1982.

Lu, L.-F., Onishi, R. and Takahashi, K.: The effect of wind on long-term summer water temperature trends in Tokyo Bay, Japan, Ocean Dyn., 65, 919-930, 2015.

Madden, R. A. and Julian, P. R.: Description of Global-Scale Circulation Cells in the Tropics with a 40–50 Day Period, J. Atmos. Sci., 29, 1109-1123, 1972.

Matsueda, M. and Endo, H.: Verification of medium-range MJO forecasts with TIGGE. Geophys. Res. Lett., 38, L11801, doi:10.1029/2011GL047480, 2011.

Mellor, G. L. and Yamada, T.: A hierarchy of turbulence closure models for planetary boundary layers. J. Atmos. Sci., 31, 1791–1806, 1974.

Mellor, G. L. and Yamada, T.: Development of a turbulence closure model for geophysical fluid problems. Rev. Geophys. Space Phys., 20, 851–875, 1982.

Miller, M. J., Palmer, T. N., and Swinbank, R.: Parameterization and influence of subgridscale orography in general circulation and numerical weather prediction models, Meteor. Atmos. Phys., 40, 84-109, 1989.

Miura, H., Satoh, M., Tomita H., Noda, A. T., Nasuno, T., and Iga, S.: A short-duration global cloud-resolving simulation with a realistic land and sea distribution, Geophys. Res. Lett., 34, L02804, doi:10.1029/2006GL027448, 2007a.

Miura, H., Satoh, M., Nasuno T., Noda, A. T., and Oouchi, K.: A Madden-Julian oscillation event realistically simulated by a global cloud-resolving model, Science, 318, 1763–1765, doi:10.1126/science.1148443, 2007b.

Miyakawa, T., Satoh, M., Miura, H., Tomita, H., Yashiro, H., Noda, A. T., Yamada, Y., Kodama, C., Kimoto, M., and Yoneyama, K.: Madden-Julian oscillation prediction skill of a new-generation global model demonstrated using a supercomputer. Nat Comm., 5: 3769. doi:10.1038/ncomms4769, 2014.

Miyamoto, K.: Introduction of the Reduced Gaussian Grid into the Operational Global NWP model at JMA. CAS/JSC WGNE Research Activities in Atmospheric and Ocean Modelling, 36, 6.9-6.10, 2006.

Miyamoto, Y., Kajikawa, Y., Yoshida, R., Yamaura, T., Yashiro, H., and Tomita, H.: Deep moist atmospheric convection in a subkilometer global simulation, Geophys. Res. Lett., 40, 4922–4926, doi:10.1002/grl.50944, 2013.

Miyamoto, Y., Yoshida, R., Yamaura T., Yashiro H., Tomita H., and Kajikawa Y.: Does convection vary in different cloud disturbances?, Atmos. Sci. Lett., 2015.

Miyoshi T., Kondo, K., and Terasaki, K.: Big Ensemble Data Assimilation in Numerical Weather Prediction, Computer, 48, 15–21; doi:10.1109/MC.2015.332, 2015.

Mizuta, R., Oouchi, K., Yoshimura, H., Noda, A, Katayama, K., Yukimoto, S., Hosaka, M., Kusunoki, S., Kawai, H., and Nakagawa, M.: 20-km-mesh global climate simulations using JMA-GSM model -- mean climate states. J. Meteor. Soc. Japan, 84, 165-185, doi:10.2151/jmsj.84.165, 2006.

Moon, I.-J., Ginis, I., Hara, T., and Thomas B.: A Physics-Based Parameterization of Air–Sea Momentum Flux at High Wind Speeds and Its Impact on Hurricane Intensity Predictions, Mon. Wea. Rev., 135, 2869-2878, 2007.

Murakami, H. and Sugi, M.: Effect of model resolution on tropical cyclone climate projections. SOLA, 6, 73-76, doi: 10.2151/sola.2010-019, 2010.

Murakami, H., Mizuta, R., and Shindo, E.: Future changes in tropical cyclone activity projected by multi-physics and multi-SST ensemble experiments using the 60-km-mesh MRI-AGCM. Clim. Dyn., 39, 2569-2584, doi: 10.1007/s00382-011-1223-x, 2012a.

Murakami, H., Wang, Y., Yoshimura, H., Mizuta, R., Sugi, M., Shindo, E., Adachi,Y., Yukimoto, S., Hosaka, M., Kusunoki, S., Ose, T., and Kitoh, A.: Future changes in tropical cyclone activity projected by the new high-resolution MRI-AGCM. J. Clim., 25, 3237-3260, doi: 10.1175/JCLI-D-11-00415.1, 2012b.

Nakanishi, M. and Niino, H.: An improved Mellor-Yamada level-3 model with condensation physics: Its design and verification. Bound.-Layer Meteor., 112, 1–31, 2004.

Nakanishi, M. and Niino, H.: An improved Mellor-Yamada level-3 model: Its numerical stability and application to a regional prediction of advection fog. Bound.-Layer Meteor., 119, 397–407, 2006.

Nakanishi, M. and Niino, H.: Development of an Improved Turbulence Closure Model for the Atmospheric Boundary Layer. J. Meteor. Soc. Japan, 87, 895–912, doi: 10.2151/jmsj.87.895, 2009.

Nakano, M., Nasuno, T., Sawada, M., and Satoh, M.: Intraseasonal variability and tropical cyclogenesis in the western North Pacific simulated by a global nonhydrostatic atmospheric model. Geophysical Research Letters, 42, 565-571, doi: 10.1002/2014GL062479, 2015.

Nasuno, T.: Forecast skill of Madden–Julian oscillation events in a global nonhydrostatic model during the CINDY2011/DYNAMO observation period. SOLA, 9, 69–73, doi: 10.2151/sola.2013-016, 2013.

Nasuno, T., Yamada, H., Nakano, M., Kubota, H., Sawada, M., and Yoshida, R.: Global cloud-permitting simulations of Typhoon Fengshen (2008), Geosci. Lett., 3:32, doi:10.1186/s40562-016-0064-1, 2016

Noda, A. T., Oouchi, K., Satoh, M., Tomita, H., Iga, S.-I., and Tsushima, Y.: Importance of the subgrid-scale turbulent moist process: Cloud distribution in global cloud-resolving simulations, Atmos Res., 96, 208–217, doi:10.1016/j.atmosres.2009.05.007, 2010.

Okamoto, K., Aonashi, K., Kubota, T., and Tashima, T.: Experimental assimilation of the GPM-Core DPR reflectivity profiles for Typhoon Halong (2014), Mon. Wea. Rev., doi: 10.1175/MWR-D-15-0399.1, 2016

Onishi, R., Takahashi, K. and Komori, S.: High-resolution simulations for turbulent clouds developing over the ocean. Gas Transfer at Water Surfaces (ed. S. Komori, W. McGillis & R. Kurose), Kyoto University Press, 6, 582–592, 2011.

Onishi, R. and Takahashi, K.: A warm-bin–cold-bulk hybrid cloud microphysical model. J. Atmos. Sci., 69, 1474–1497. doi: 10.1175/JAS-D-11-0166.1, 2012.

書式変更

Onogi, K., Tsutsui, J., Koide, H., Sakamoto, M., Kobayashi, S., Hatsushika, H., Matsumoto, T., Yamazaki, N., Kamahori, H., Takahashi, K., Kadokura, S., Wada, K., Kato, K., Oyama, R., Ose, T., Mannoji, N., and Taira, R.: The JRA-25 Reanalysis, J. Meteor. Soc. Jpn., 85, 369-432, doi: 10.2151/jmsj.85.369, 2007

Oouchi, K., Noda, A. T., Satoh, M., Miura, H., Tomita, H., Nasuno,T., Iga, S.: A simulated preconditioning of typhoon genesis controlled by a boreal summer Madden-Julian Oscillation event in a global cloud-resolving mode.SOLA, 5, 65-68, doi: doi:10.2151/sola.2009-017, 2009.

Priestley, A.: A quasi-conservative version of the semi-Lagrangian advection scheme. Mon. Wea. Rev., 121, 621-629, 1993.

Randall, D. and Pan, D.-M.: Implementation of the Arakawa-Schubert cumulus parameterization with a prognostic closure. The representation of cumulus convection in numerical models, AMS Meteor. Monogr. Series, 46, 137–144, 1993.

Randall, D., Khairoutdinov, M., Arakawa, A., and Grabowski, W.: Breaking the Cloud Parameterization Deadlock. Bull. Amer. Meteorol. Soc., 84, 1547–1564, doi: 10.1175/BAMS-84-11-1547, 2003.

Rogers, R. F., Reasor, P. and Lorsolo, S.: Airborne doppler observations of the inner-core structural differences between intensifying and steady-state tropical cyclones. Mon. Wea. Rev., 141, 2970-2991, 2013.

Peng, X., Xiao, F. and Takahashi, K.: Conservation constraint for quasi-uniform overset grid on sphere. Quart. J. Roy. Meteor. Soc., 132, pp.979–996, 2006.

Sasaki, W., R. Onishi, R., H. Fuchigami, H.,, K. Goto, K., S. Nishikawa, S., Y. Ishikawa, Y., and K. Takahashi, K. : (2016) : MJO simulation in a cloud-system-resolving global ocean-atmosphere coupled model, Geophys. Res. Lett., 43, 9352–9360, doi:10.1002/2016GL070550, 2016 .

Satoh, M., Matsuno, T., Tomita, H., Miura, H., Nasuno, T. and Iga, S.: Nonhydrostatic icosahedral atmospheric model (NICAM) for global cloud resolving simulations. J. Comput. Phys., 227, 3486-3514, 2008.

Satoh, M., Tomita, H., Yashiro, H., Miura, H, Kodama, C., Seiki, T., Noda, A. T., Yamada, Y., Goto, D., Sawada, M., Miyoshi, T., Niwa, Y., Hara, M., Ohno, T., Iga, S., Arakawa, T., Inoue, T. and Kubokawa, H.: The non-hydrostatic icosahedral atmospheric model: description and development. Progress in Earth and Planetary Science, 1:18, 2014.

Sekiguchi, M. and Nakajima, T.: A k-distribution-based radiation code and its computational optimization for an atmospheric general circulation model. J. Quant. Spectrosc. Radiat. Transfer, 109, 2779-2793, 2008.

Shibata, K., Yoshimura, H., Ohizumi, M., Hosaka, M. and Sugi, M.: A simulation of troposphere, stratosphere and mesosphere with MRI/JMA98 GCM. Pap. Meteor. Geophys., 50(1), 15-53, 1999.

Shapiro, L. J., and Willoughby, H. E.: The response of balanced hurricanes to local sources of heat and momentum, J. Atmos. Sci., 39, 378-394, 1982

Skamarock, W. C.: Evaluating mesoscale NWP models using kinetic energy spectra. Mon. Wea. Rev., 132, 3019–3032, doi:10.1175/MWR2830.1, 2004.

Smith, R. N. B.: A scheme for predicting layer clouds and their water content in a general circulation model. Quart. J. Roy. Meteor. Soc., 116, 435–460, 1990.

Stern, D. P., Vigh, J. L., Nolan, D. S., and Zhang, F.: Revisiting the Relationship Between Eyewall Contraction and Intensification. J. Atmos. Sci., 72, 1283–1306, doi:10.1175/JAS-D-14-0261.1, 2015.

Takahashi, K., Peng, X., Ohnishi, R., Sugimura, T., Ohdaira, M., Goto, K. and Fuchigami, H.: Multi-Scale Weather/Climate Simulations with Multi-Scale Simulator for the Geoenvironment (MSSG) on the Earth Simulator. Ann. Rep. Earth Simulator Center, April 2006–March 2007, pp.27–33, ISSN 1348–5822, 2006.

Takahashi K., Onishi R., Baba Y., Kida S., Matsuda K., Goto, K. and Fuchigami, H.: Challenge toward the prediction of typhoon behaviour and down pour. J. Phys.: Conference Series 454:012,072, 2013.

Toro, E. F.: A weighted average flux method for hyperbolic conservation laws. Proc. Roy. Soc. London, A423, 401–418, 1989.

書式変更：英語（英国）
書式変更：英語（英国）
書式変更：英語（英国）
書式変更：英語（英国）
書式変更：英語（英国）
書式変更：英語（英国）
書式変更：英語（英国）
書式変更：英語（英国）
書式変更：英語（英国）

Takata, K, Emori, S., and Watanabe, T.: Development of the minimal advanced treatments of surface interaction and runoff. Global and Planet. Change, 38, 209-222, 2003.

Taniguchi, H., Yanase, W., and Satoh, M.: Ensemble Simulation of Cyclone Nargis by a Global Cloud-System-Resolving Model—Modulation of Cyclogenesis by the Madden-Julian Oscillation, J. Meteor. Soc. Jpn., 88, 571-591, doi: 10.2151/jmsj.2010-317, 2010.

Tomita, H., Tsugawa, M., Satoh, M., and Goto, K.: Shallow Water Model on a Modified Icosahedral Geodesic Grid by Using Spring Dynamics, J. Comp. Phys., 174, 579-613, doi:10.1006/jcph.2001.6897, 2001

Tomita, H.: New microphysical schemes with five and six categories by diagnostic generation of cloud ice, J. Meteorol. Soc. Japan, 86A, 121-142. doi: 10.2151/jmsj.86A.121, 2008.

Wang, B., and Rui, H.: Synoptic climatology of transient tropical intraseasonal convection anomalies: 1975–1985, Meteorol. Atmos. Phys., 44, 43–61, 1990.

Wang, B., and Xie, X.: A model for the boreal summer intraseasonal oscillation, J. Atmos. Sci., 54, 72–86, 1997.

Wang, H., and Wang, Y.: A numerical study of typhoon Megi (2010): Part I: Rapid intensification. Mon. Wea. Rev., 142, 29-48, doi:10.1175/MWR-D-13-00070.1, 2014.

Wedi, N. P. and Smolarkiewicz, P. K.: A framework for testing global non-hydrostatic models. Q. J. R. Meteor. Soc., 135, 469-484, doi: 10.1002/qj.377, 2009.

Wicker, L. J. and Skamarock, W.C.: Time-split-ting methods for elastic models using forward time schemes, Monthly Weather Review, 130, 2088–2097, 2002.

Xiang, B., Lin, S.-J., Zhao, M., Zhang, S., Vecchi, G., Li, T., Jiang, X., Harris, L., and Chen, J.-H.: Beyond weather time-scale prediction for hurricane Sandy and super typhoon Haiyan in a global climate model. Mon. Wea. Rev., 143, 524-535, doi: 10.1175/MWR-D-14-00227.1, 2015.

Yablonsky, R. M., and Genis, I.: Limitation of One-Dimensional Ocean Models for Coupled Hurricane–Ocean Model Forecasts, Mon. Wea. Rev., 137, 4410–4419, doi: 10.1175/2009MWR2863.1, 2009.

Yabu, S.: Development of longwave radiation scheme with consideration of scattering by clouds in JMA global model, CAS/JSC WGNE Research Activities in Atmospheric and Oceanic Modelling. 43. 4.07-4.08, 2013.

Yamada H, Nasuno T, Yanase W, and Satoh M: Role of the vertical structure of a simulated tropical cyclone in its motion: A case study of Typhoon Fengshen (2008), SOLA, 12, 203–208, doi: 10.2151/sola.2016-041041~~accepted~~, 2016.

Yamaguchi, M., Iriguchi, T., Nakazawa, T., and Wu, C.-C.: An observing system experiment for Typhoon Conson (2004) using a singular vector method and DOTSTAR data. Mon. Wea. Rev., 137, 2801-2816, 2009.

Yamaguchi, M., Nakazawa, T. and Hoshino, S.: On the relative benefits of a multi-centre grand ensemble for tropical cyclone track prediction in the western North Pacific. Quart. J. Roy. Meteor. Soc., 138, 2019–2029, doi:10.1002/qj.1937, 2012.

Yamaguchi, M., Vitart, F., Lang, S. T. K., Magnusson, L., Elsberry, R. L., Elliott, G., Kyouda, M., and Nakazawa, T.: Global distribution on the skill of tropical cyclone activity forecasts from short- to medium-range time scales. Wea. Forecast, 30, 1695-1709, doi: 10.1175/WAF-D-14-00136.1, 2015.

Yanase, W., Taniguchi, H., and Satoh, M.: The genesis of tropical cyclone Nargis (2008): Environmental modulation and numerical predictability. J. Meteor. Soc. Japan, 88, 497-519, doi: 10.2151/jmsj.2010-314, 2010.

Yoshimura, H. and Matsumura, T.: A Semi-Lagrangian Scheme Conservative in the Vertical Direction. CAS/JSC WGNE Research Activities in Atmospheric and Ocean Modeling, 33, 3.19-3.20, 2003.

Yoshimura, H. and Matsumura, T.: A two-time-level vertically-conservative semi-Lagrangian semi-implicit double Fourier series AGCM. CAS/JSC WGNE Research Activities in Atmospheric and Ocean Modeling, 35, 3.25-3.26, 2005.

Yoshimura, H.: Development of a nonhydrostatic global spectral atmospheric model using double Fourier series. CAS/JSC WGNE Research Activities in Atmospheric and Ocean Modeling, 42, 3.05-3.06, 2012.

Yukimoto, S., and Coauthors: Meteorological Research Institute-Earth System Model Version 1 (MRI-ESM1) —) –Model Description–. Technical Reports of the Meteorological Research Institute, No. 64, 2011.

Zhang, D. and Anthes, R. A.: A high-resolution model of the planetary boundary layer—sensitivity tests and comparisons with SESAME-79 Data. J. Appl. Meteor., 21, 1594–1609, 1982.

Zhang, F., Minamide, M., and Clothiaux, E. E.: Potential impacts of assimilating all-sky infrared satellite radiances from GOES-R on convection-permitting analysis and prediction of tropical cyclones, Geophys. Res. Lett., 43, 2954–2963, doi:10.1002/2016GL068468, 2016.

Table 1. List of initial times for stage 1 of TYMIP-G7.

	Initial time	Typhoon case (*Italic*: weaker than Tropical Storm, ***Bold italic***: ***extratropical cyclone***)	DFSM	GSM	MSSG	NICAM
1	12 September 2013, 00:00:00 UTC	*Man-yi*	○	○	○	○
2	12 September 2013, 06:00:00 UTC	*Man-yi*	○	○	○	○
3	12 September 2013, 12:00:00 UTC	*Man-yi*	○	○	○	○
4	12 September 2013, 18:00:00 UTC	*Man-yi*	○	○	○	○
5	13 September 2013, 00:00:00 UTC	Man-yi	○	○	○	○
6	30 September 2013, 00:00:00 UTC	Wutip, Sepat, *Fitow*	○	○	○	○
7	30 September 2013, 06:00:00 UTC	Wutip, Sepat, *Fitow*	○	○	○	○(*1)
8	30 September 2013, 12:00:00 UTC	Wutip, Sepat, *Fitow*	○	○	○	○
9	30 September 2013, 18:00:00 UTC	Wutip, Sepat, *Fitow*	○	○	○	○
10	1 October 2013, 00:00:00 UTC	***Wutip***, Sepat, Fitow, *Danas*	○	○	○	○
11	1 October 2013, 06:00:00 UTC	Sepat, Fitow, *Danas*	○	○	○	○(*1)
12	1 October 2013, 12:00:00 UTC	Sepat, Fitow, *Danas*	○	○	○	○(*1)
13	1 October 2013, 18:00:00 UTC	Sepat, Fitow, *Danas*	○	○	○	○(*1)
14	2 October 2013, 00:00:00 UTC	Sepat, Fitow, *Danas*	○	○	○	○(*1)
15	2 October 2013, 06:00:00 UTC	Sepat, Fitow, *Danas*	○	○	○	○
16	2 October 2013, 12:00:00 UTC	Sepat, Fitow, *Danas*	○	○	○	○
17	2 October 2013, 18:00:00 UTC	***Sepat***, Fitow, *Danas*	○	○	○	○(*1)
18	3 October 2013, 00:00:00 UTC	***Sepat***, Fitow, *Danas*	○	○	○	○
19	3 October 2013, 06:00:00 UTC	***Sepat***, Fitow, *Danas*	○	○	○	○
20	3 October 2013, 12:00:00 UTC	***Sepat***, Fitow, *Danas*	○	○	○	○
21	3 October 2013, 18:00:00 UTC	***Sepat***, Fitow, *Danas*	○	○	○	○(*1)
22	4 October 2013, 00:00:00 UTC	Fitow, *Danas*	○	○	○	○(*1)
23	9 October 2013, 00:00:00 UTC	***Danas***,*Nari*,*Wipha*	○	○	○	○
24	9 October 2013, 06:00:00 UTC	***Danas***,*Nari*,*Wipha*	○	○	○	○
25	9 October 2013, 12:00:00 UTC	Nari,*Wipha*	○	○	○	○
26	9 October 2013, 18:00:00 UTC	Nari,*Wipha*	○	○	○	○
27	10 October 2013, 00:00:00 UTC	Nari,*Wipha*	○	○	○	○
28	10 October 2013, 06:00:00 UTC	Nari,*Wipha*	○	○	○	○
29	10 October 2013, 12:00:00 UTC	Nari,Wipha	○	○	○	○
30	10 October 2013, 18:00:00 UTC	Nari,Wipha	○	○	○	○
31	11 October 2013, 00:00:00 UTC	Nari,Wipha	○	○	○	○
32	11 October 2013, 06:00:00 UTC	Nari,Wipha	○	○	○	○
33	11 October 2013, 12:00:00 UTC	Nari,Wipha	○	○	○	○
34	11 October 2013, 18:00:00 UTC	Nari,Wipha	○	○	○	○
35	12 October 2013, 00:00:00 UTC	Nari,Wipha	○	○	○	○
36	12 October 2013, 06:00:00 UTC	Nari,Wipha	○	○	○	○
37	12 October 2013, 12:00:00 UTC	Nari,Wipha	○	○	○	○
38	17 October 2013, 12:00:00 UTC	***Wipha***, Francisco	○	○	○	○
39	17 October 2013, 18:00:00 UTC	***Wipha***, Francisco	○	○	○	○
40	18 October 2013, 00:00:00 UTC	***Wipha***, Francisco	○	○	○	○
41	18 October 2013, 06:00:00 UTC	***Wipha***, Francisco	○	○	○	○
42	18 October 2013, 12:00:00 UTC	***Wipha***, Francisco	○	○	○	○(*1)
43	18 October 2013, 18:00:00 UTC	Francisco	○	○	○	○

44	19 October 2013, 00:00:00 UTC	Francisco, *Lekima*	○	○	○	○(*1)
45	19 October 2013, 06:00:00 UTC	Francisco, *Lekima*	○	○	○	○
46	19 October 2013, 12:00:00 UTC	Francisco, *Lekima*	○	○	○	○
47	19 October 2013, 18:00:00 UTC	Francisco, *Lekima*	○	○	○	○
48	20 October 2013, 00:00:00 UTC	Francisco, *Lekima*	○	○	○	○
49	20 October 2013, 06:00:00 UTC	Francisco, *Lekima*	○	○	○	○
50	20 October 2013, 12:00:00 UTC	Francisco, *Lekima*	○	○	○	○(*1)
51	20 October 2013, 18:00:00 UTC	Francisco, *Lekima*	○	○	○	○
52	21 October 2013, 00:00:00 UTC	Francisco, *Lekima*	○	○	○	○

(*1): rerun with the fixed version of MATSIRO (Sect. 2.2.3~~)~~).

Table 2 ~~Same as Table 1, but~~. List of initial times for stage 2 of TYMIP-G7.

	Initial time	Typhoon case (*Italic*: weaker than Tropical Storm, ***Bold italic***: ***extratropical cyclone***) and MJO/BSISO case	DFSM	GSM	MSSG	NICAM (*2)
1	6 June 2013, 12:00:00 UTC	*Yagi*	○	○	○	○
2	7 June 2013, 00:00:00 UTC	*Yagi*	○	○	○	○
3	7 June 2013, 12:00:00 UTC	*Yagi*	○	○	○	○
4	8 June 2013, 00:00:00 UTC	*Yagi*	○	○	○	○
5	8 June 2013, 12:00:00 UTC	Yagi	○	○	○	○
6	9 June 2013, 00:00:00 UTC	Yagi	○	○	○	○
7	9 June 2013, 12:00:00 UTC	Yagi	○	○	○	○
8	10 June 2013, 00:00:00 UTC	Yagi	○	○	○	○
9	10 June 2013, 12:00:00 UTC	Yagi	○	○	○	○
10	11 June 2013, 00:00:00 UTC	Yagi	○	○	○	○
11	3 November 2013, 00:00:00 UTC	Krosa	○	○	○	○
12	3 November 2013, 12:00:00 UTC	Krosa, *Haiyan*	○	○	○	○
13	4 November 2013, 00:00:00 UTC	Krosa, Haiyan	○	○	○	○
14	4 November 2013, 12:00:00 UTC	***Krosa***, Haiyan	○	○	○	○
15	5 November 2013, 00:00:00 UTC	Haiyan	○	○	○	○
16	5 November 2013, 12:00:00 UTC	Haiyan	○	○	○	○
17	6 November 2013, 00:00:00 UTC	Haiyan	○	○	○	○
18	6 November 2013, 12:00:00 UTC	Haiyan	○	○	○	○
19	7 November 2013, 00:00:00 UTC	Haiyan	○	○	○	○
20	27 July 2014, 12:00:00 UTC	*Halong*	○	○	○	○
21	28 July 2014, 00:00:00 UTC	*Halong*	○	○	○	○
22	28 July 2014, 12:00:00 UTC	*Halong*, *Nakri*	○	○	○	○
23	29 July 2014, 00:00:00 UTC	Halong, *Nakri*	○	○	○	○
24	29 July 2014, 12:00:00 UTC	Halong, Nakri	○	○	○	○
25	30 July 2014, 00:00:00 UTC	Halong, Nakri	○	○	○	○
26	30 July 2014, 12:00:00 UTC	Halong, Nakri	○	○	○	○
27	31 July 2014, 00:00:00 UTC	Halong, Nakri	○	○	○	○
28	31 July 2014, 12:00:00 UTC	Halong, Nakri	○	○	○	○
29	1 August 2014, 00:00:00 UTC	Halong, Nakri	○	○	○	○
30	1 August 2014, 12:00:00 UTC	Halong, Nakri	○	○	○	○
31	2 August 2014, 00:00:00 UTC	Halong, Nakri	○	○	○	○
32	2 August 2014, 12:00:00 UTC	Halong, Nakri	○	○	○	○
33	3 August 2014, 00:00:00 UTC	Halong, Nakri	○	○	○	○
34	3 August 2014, 12:00:00 UTC	Halong, *Nakri*	○	○	○	○
35	4 August 2014, 00:00:00 UTC	Halong, *Nakri*	○	○	○	○
36	4 August 2014, 12:00:00 UTC	Halong	○	○	○	~~×~~
37	5 August 2014, 00:00:00 UTC	Halong	○	○	○	~~×~~
38	5 August 2014, 12:00:00 UTC	Halong	○	○	○	○
39	6 August 2014, 00:00:00 UTC	Halong	○	○	○	○
40	6 August 2014, 12:00:00 UTC	Halong	○	○	○	○
41	7 March 2015, 00:00:00 UTC	MJO	○	○	○	○
42	7 March 2015, 12:00:00 UTC	MJO	○	○	○	○
43	8 March 2015, 00:00:00 UTC	MJO	○	○	○	○
44	8 March 2015, 12:00:00 UTC	MJO	○	○	○	○
45	9 March 2015, 00:00:00 UTC	MJO	○	○	○	○
46	9 March 2015, 12:00:00 UTC	MJO, Pam	○	○	○	○
47	10 March 2015, 00:00:00 UTC	MJO, Pam	○	○	○	○
48	10 March 2015, 12:00:00 UTC	MJO, *Bavi*, Pam	○	○	○	○
49	11 March 2015, 00:00:00 UTC	MJO, *Bavi*, Pam	○	○	○	○
50	11 March 2015, 12:00:00 UTC	MJO, Bavi, Pam	○	○	○	○
51	27 June 2015, 00:00:00 UTC	BSISO	○	○	○	○
52	27 June 2015, 12:00:00 UTC	BSISO	○	○	○	○
53	28 June 2015, 00:00:00 UTC	BSISO	○	○	○	○
54	28 June 2015, 12:00:00 UTC	BSISO	○	○	○	○

書式変更

55	29 June 2015, 00:00:00 UTC	BSISO	○	○	○	○
56	29 June 2015, 12:00:00 UTC	BSISO,*Chan-hom*	○	○	○	○
57	30 June 2015, 00:00:00 UTC	BSISO,*Chan-hom*	○	○	○	○
58	30 June 2015, 12:00:00 UTC	BSISO,Chan-hom	○	○	○	○
59	1 July 2015, 00:00:00 UTC	BSISO,Chan-hom	○	○	○	○
60	1 July 2015, 12:00:00 UTC	BSISO,Chan-hom	○	○	○	○
61	13 August 2015, 12:00:00 UTC		○	○	○	○
62	14 August 2015, 00:00:00 UTC	***Molave,*** *Goni, Atsani*	○	○	○	○
63	14 August 2015, 12:00:00 UTC	***Molave,*** *Goni, Atsani*	○	○	○	○
64	15 August 2015, 00:00:00 UTC	***Molave,*** Goni, Atsani	○	○	○	○
65	15 August 2015, 12:00:00 UTC	***Molave,*** Goni, Atsani	○	○	○	○
66	16 August 2015, 00:00:00 UTC	***Molave,*** Goni, Atsani	○	○	○	○
67	16 August 2015, 12:00:00 UTC	***Molave,*** Goni, Atsani	○	○	○	○
68	17 August 2015, 00:00:00 UTC	***Molave,*** Goni, Atsani	○	○	○	○
69	17 August 2015, 12:00:00 UTC	***Molave,*** Goni, Atsani	○	○	○	○
70	18 August 2015, 00:00:00 UTC	***Molave,*** Goni, Atsani	○	○	○	○
71	18 August 2015, 12:00:00 UTC	Goni, Atsani	○	○	○	○
72	19 August 2015, 00:00:00 UTC	Goni, Atsani	○	○	○	○
73	19 August 2015, 12:00:00 UTC	Goni, Atsani	○	○	○	○
74	20 August 2015, 00:00:00 UTC	Goni, Atsani	○	○	○	○
75	20 August 2015, 12:00:00 UTC	Goni, Atsani	○	○	○	○
76	21 August 2015, 00:00:00 UTC	Goni, Atsani	○	○	○	○
77	6 September 2015, 00:00:00 UTC	Kilo, *Etau*	○	○	○	○
78	6 September 2015, 12:00:00 UTC	Kilo, *Etau*	○	○	○	○
79	7 September 2015, 00:00:00 UTC	Kilo, *Etau*	○	○	○	○
80	7 September 2015, 12:00:00 UTC	Kilo, Etau	○	○	○	○
81	8 September 2015, 00:00:00 UTC	Kilo, Etau	○	○	○	○
82	8 September 2015, 12:00:00 UTC	Kilo, Etau	○	○	○	○
83	9 September 2015, 00:00:00 UTC	Kilo, Etau	○	○	○	○
84	9 September 2015, 12:00:00 UTC	Kilo, ***Etau***	○	○	○	○
85	10 September 2015, 00:00:00 UTC	Kilo, ***Etau***	○	○	○	○

(*2): run with the fixed version of MATSIRO (Sect. 2.2.3~~)~~).

書式変更

Table 3. Output variables and domains.

Domain	Interval	Variable	Horizontal resolution
Global	1 hour	Accumulated cloud ice (*cldi*), Accumulated cloud water (*cldw*), Outward longwave radiation (*olr*), Sea-level pressure (*psea*), 2-m specific humidity (*qs*), Sea surface temperature (*sst*), Total precipitable water (*tpw*), 2-m temperature (*ts*), 10-m zonal wind speed (*us*), 10-m meridional wind speed (*vs*)	1.25°
	1 hour (average)	Latent heat flux (*fllh*), Zonal wind stress (*flmu*), Meridional wind stress (*flmv*), Sensible heat flux (*flsh*), Precipitation (*prc*), Precipitation by cumulus parameterization (*prcc*)	1.25°
	3 hours	Cloud cover (*cvr*), Cloud water content (*cwc*), Cloud water (*qc* or *xc*), Cloud ice (*qi* or *xi*), rain water (*qr* or *xr*), snow (*qs* or *xs*), graupel (*qg* or *xg*), Specific humidity (*q*), Relative humidity (*rh*), Temperature (*t*), Zonal wind speed (*u*), Meridional wind speed (*v*), Vertical wind speed (*w*), Height (*z*)	1.25°
	3 hours (average)	Cumulus-induced heating (*hrcv*), Cloud-induced heating (*hrlc*), Radiation-induced heating (*hrr*), Turbulence-induced heating (*hrvd*), Cumulus-induced moistening (*qrcv*), Cloud-induced moistening (*qrlc*), Radiation-induced heating (*qrvd*), Cumulus-induced zonal acceleration (*urcv*), Turbulence-induced zonal acceleration (*urvd*), Cumulus-induced meridional acceleration (*vrcv*), Turbulence-induced meridional acceleration (*vrvd*)	1.25°
Western North Pacific/Tropics	1 hour	cldi, cldw, olr, psea, qs, sst, tpw, ts, us, vs	~7 km
	1 hour (average)	fllh, flmu, flmv, flsh, prc, prcc	~7 km
	3 hours	cvr, cwc, q, rh, t, u. v, w, z	~7 km
	3 hours (average)	hrcv, hrlc, hrr, hrvd, qrcv, qrlc, qrvd, urcv, urvd, vrcv, vrvd	~7 km

書式変更

Table 4. Brief description of ~~specification~~the specifications for each global nonhydrostatic model.

	DFSM	GSM	MSSG	NICAM
Horizontal resolution	7 km	20 km	7 km	7 km
Horizontal Grid configuration	Reduced linear equally-spaced latitude grid	Reduced linear Gaussian grid	Yin-yang grid	Icosahedral grid
Number of grids in horizontal direction	8845592	1312360	11184128	10485760
Vertical coordinate	Hybrid sigma-pressure coordinate	Hybrid sigma-pressure coordinate	Terrain-following coordinate	Terrain-following coordinate
Vertical levels	100 (top: 0.01 hPa, bottom: 999.0429 hPa (*3) ~~(about 8m~~(~8 m))	100 (top: 0.01 hPa, bottom: 999.0429 hPa (*3) ~~(about 8m~~(~8 m))	55 (top: 40 km, bottom: ~~75m~~75 m)	38 (top: 36.7 km, bottom: 80 m)
Dynamical core	Nonhydrostatic spectral model using double Fourier series	Hydrostatic spectral model using spherical harmonics	Nonhydrostatic grid model using finite difference method	Nonhydrostatic grid model using finite volume method
Time step (s)	200	400	Variable	30
Cloud physics	Smith (1990)	Smith (1990)	Onishi ~~&~~and Takahashi (2012)	Tomita (2008)
Cumulus convection	Randall ~~&~~and Pan (1993)	Randall ~~&~~and Pan (1993)	Not used	Not used
Planetary boundary layer	MY2 (Mellor ~~&~~and Yamada, 1974, 1982)	MY2 (Mellor ~~&~~and Yamada, 1974, 1982)	MYNN2.5 (Nakanishi ~~&~~and Niino, 2009)	MYNN2 (Nakanishi ~~&~~and Niino, 2004; Noda et al~~.~~., 2010)
Radiation	JMA (2013), Yabu (2013)	JMA (2013), Yabu (2013)	MstranX (Sekiguchi ~~&~~and Nakajima, 2008)	MstranX (Sekiguchi ~~&~~and Nakajima, 2008)
Land and ocean	SiB (JMA, 2013)	SiB (JMA, 2013)	Bucket ~~(~~Option: 3D ocean model~~)~~	MATSIRO (Takata et al~~.~~., 2003) Slab ocean model
Surface boundary layer	Louis (1982), Miller (1989, Ocean/ Unstable atmosphere)	Louis (1982), Miller (1989, Ocean/ Unstable atmosphere)	Zhang ~~&~~and Anthes (1982) for land surface; Fairall et al. (1996; 2003) for ocean surface	Louis (1979)

(*3): Full-level pressure for surface pressure = 1000 hPa.

書式変更

Table 5 Computational performance in 12 September 2013, 00:00:00 UTC case

Model	Time step (s)	Number of nodes	Elapse time (sec) (including output of model data)	Node×hours	Execution efficiency (%)
DFSM	200	320	7673	682	4.0
MSSG	17.7	512	16381	2330	15.1
NICAM	30	640	6497	1155	16.5
GSM	400	10	5896	16.4	16.0

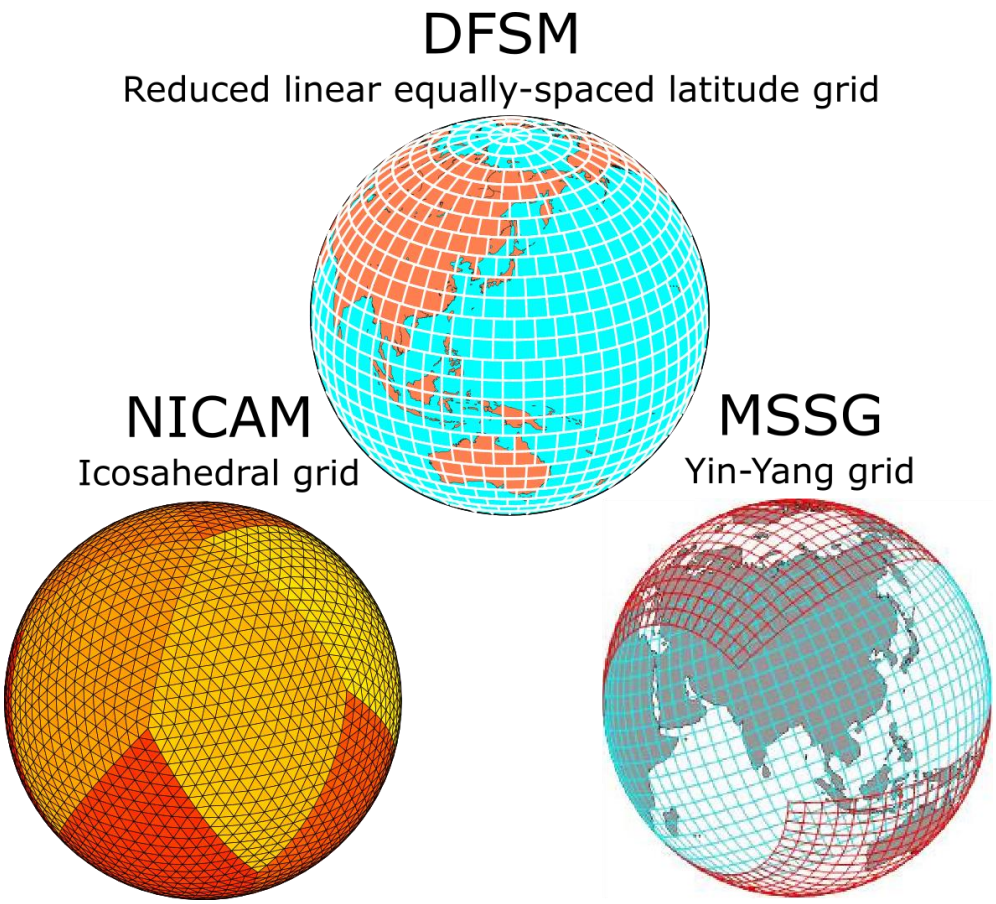

Figure 1: Schematic diagram of the horizontal grid structures of the three models used in TYMIP-G7.

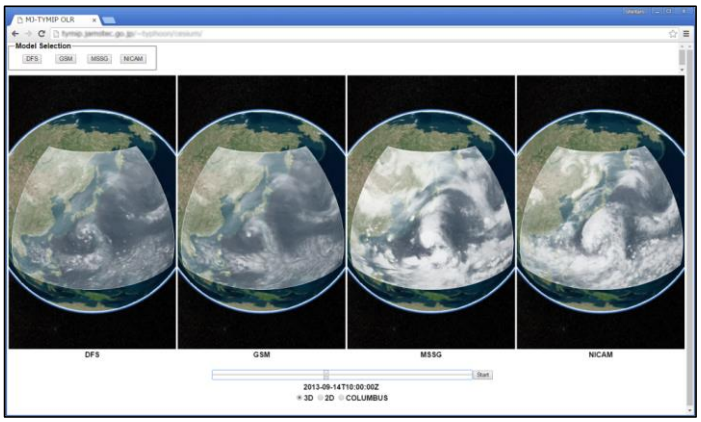

Figure 2~~:~~. Screen capture of the Web application: outgoing longwave radiation at 14 September 2013, 10:00:00 UTC simulated in experiments initialized at 12 September 2013, 06:00:00 UTC.

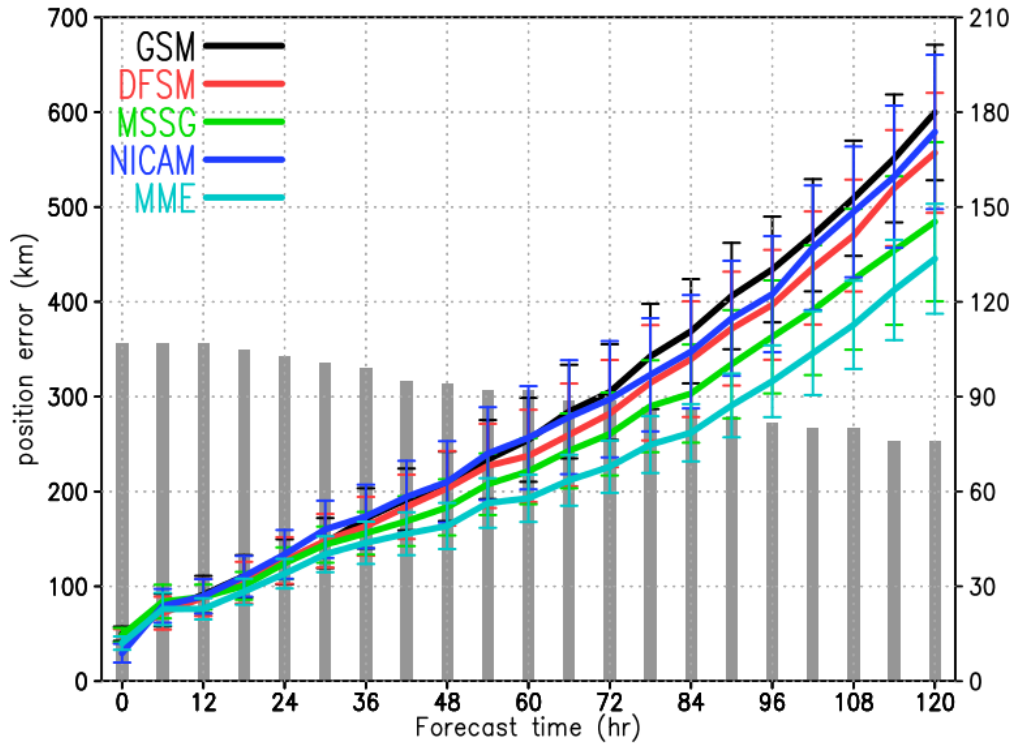

書式変更: 英語（英国），スペル チェックと文章校正を行う

書式変更: フォント：（日）ＭＳ 明朝

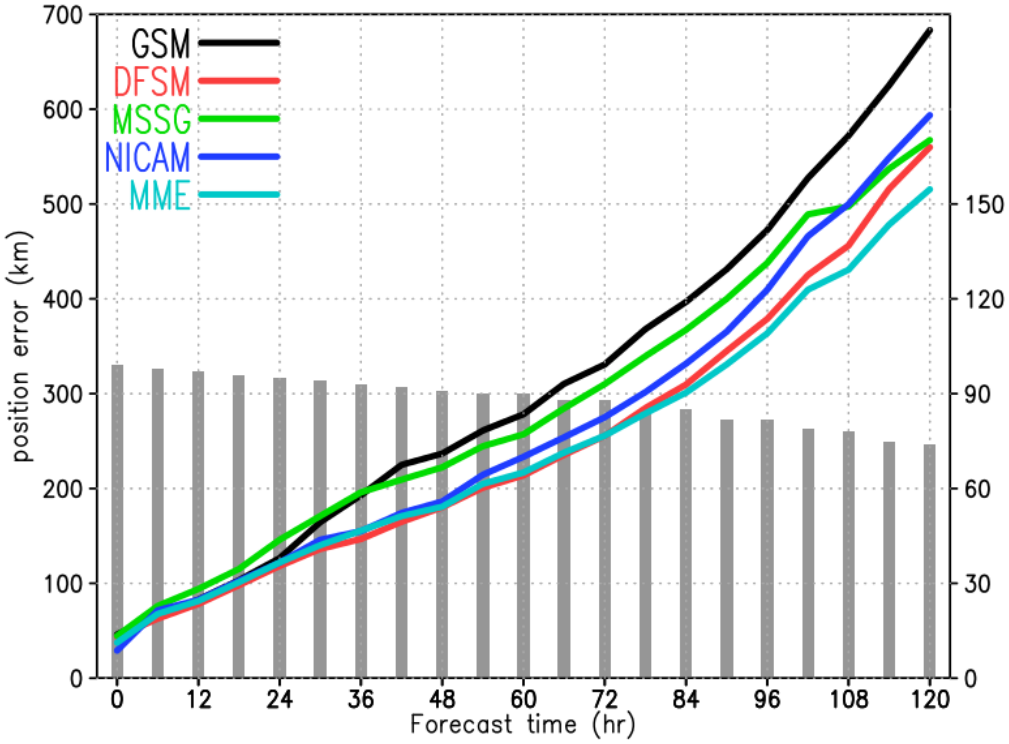

Figure 3. Errors in the track prediction for GSM, DFSM, MSSG, NICAM and MME (in the second stage). Each grey bar indicates the number of samples at each forecast time (right–vertical axis). Error bars indicate 95% confidence levels of the central pressure difference between the prediction and the RSMC Tokyo best–track data.

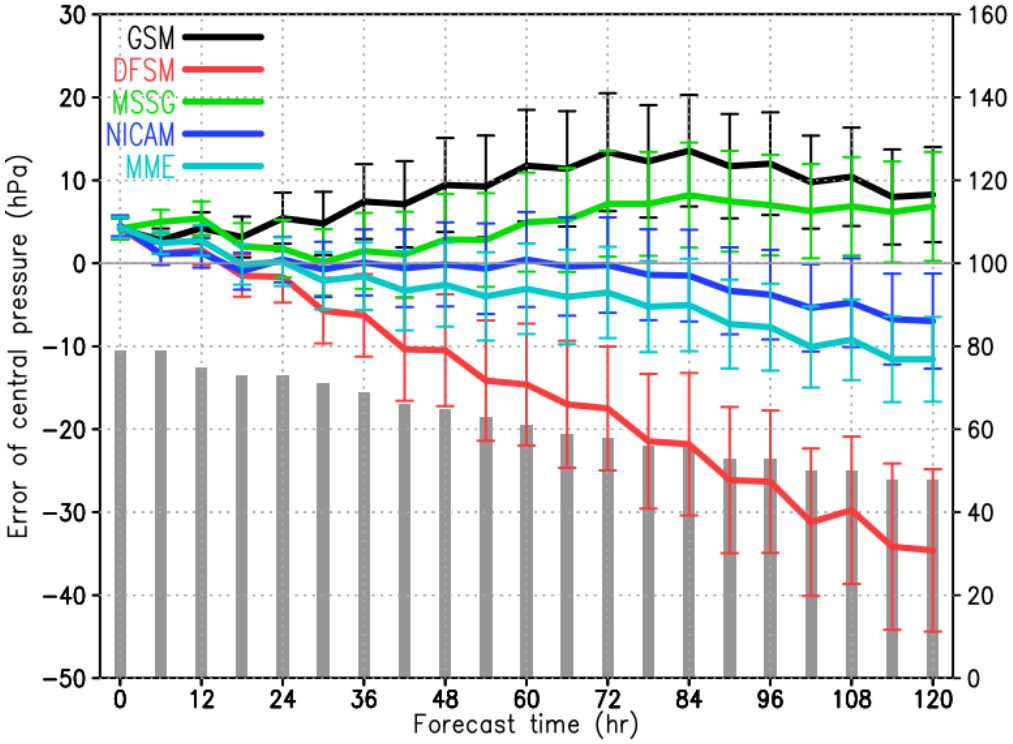
GSM
DFSM
MSSG
NICAM
MME
Error of central pressure (hPa)
Forecast time (hr)
30
20
10
0
−10
−20
−30
−40
−50
160
140
120
100
80
60
40
20
0
0
12
24
36
48
60
72
84
96
108
120

書式変更：英語（英国）

書式変更: フォント：（日）ＭＳ 明朝

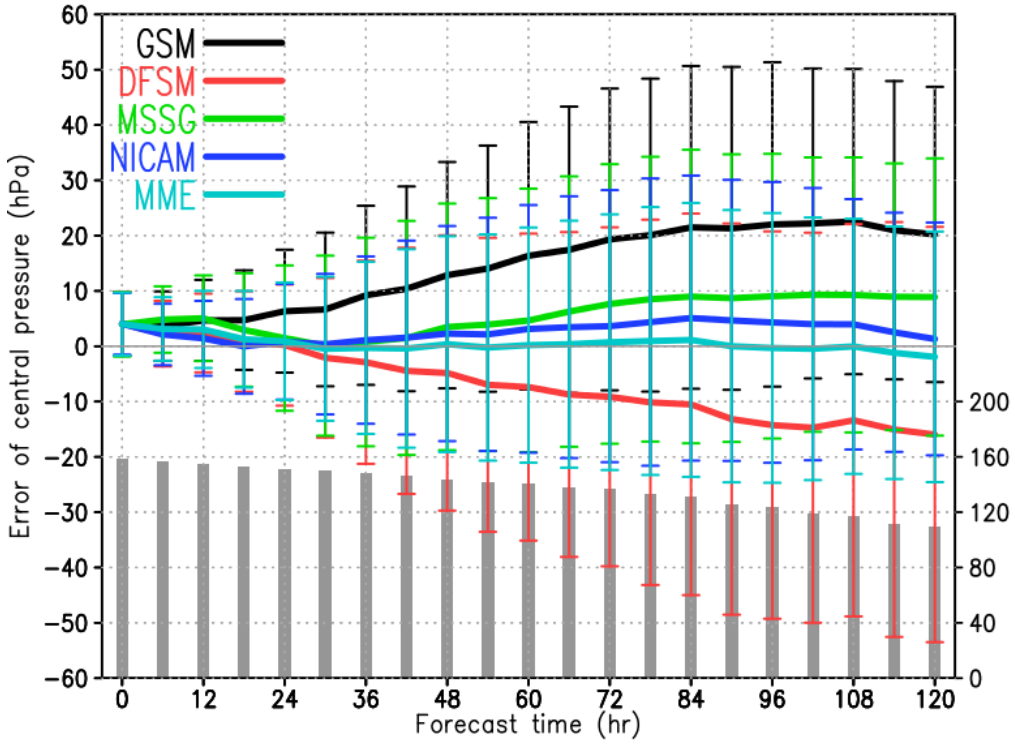

Figure 4. Errors in the predictions of the central pressure for GSM, DFSM, MSSG, NICAM and MME (in the second stage). Each grey bar indicates the number of samples at each forecast time (right–vertical axis). Error bars indicate ~~standard deviation~~95% confidence levels of the central pressure difference between the prediction and the RSMC Tokyo~~JMA~~ best–track data.

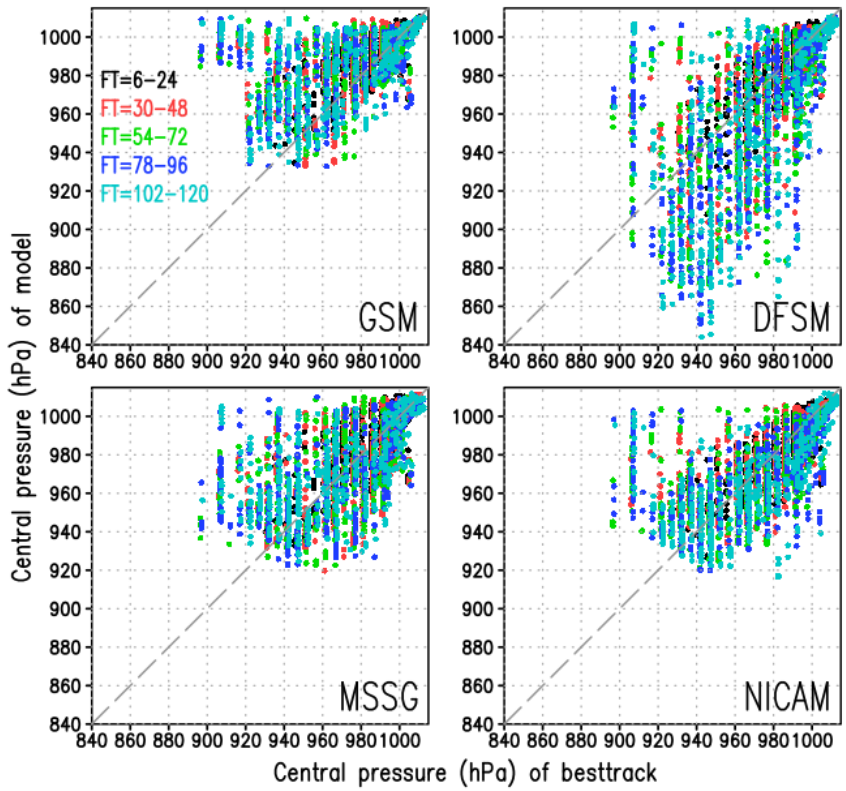

書式変更: フォント：（日）ＭＳ 明朝

書式変更: 英語（英国），スペル チェックと文章校正を行う

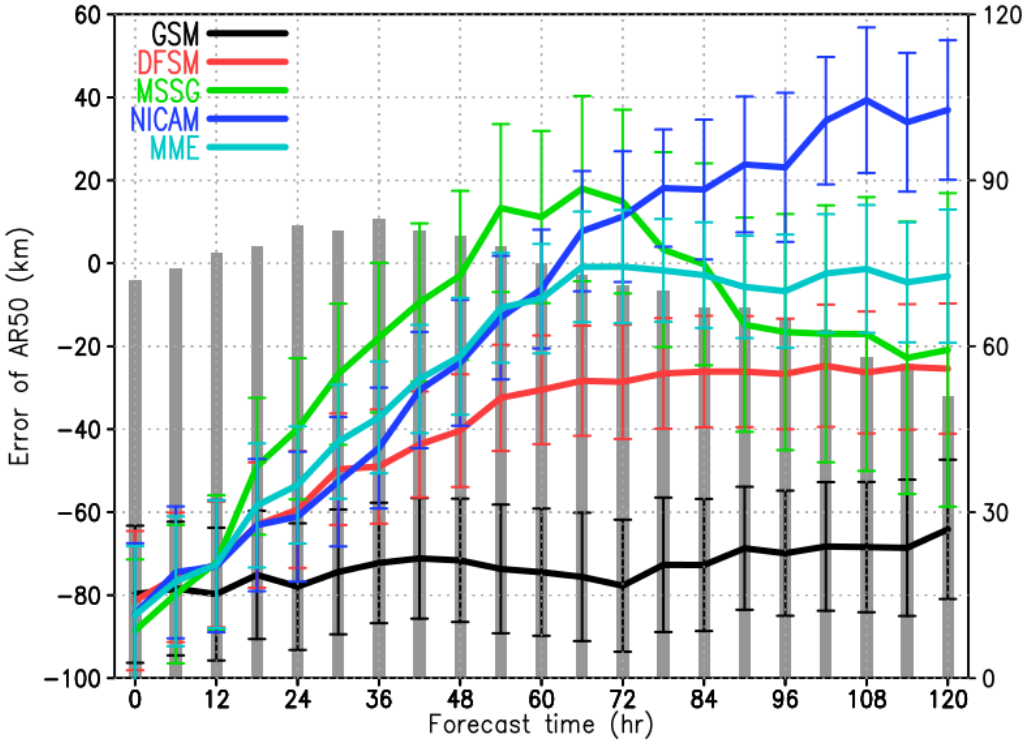

Figure 5. Errors in the averaged radius of the 50-knot wind (AR50) for GSM, DFSM, MSSG, NICAM and MME (in the second stage). Each grey bar indicates the number of samples at each forecast time (right-vertical axis). Error bars indicate 95% confidence levels of the AR50 difference between the prediction and the RSMC Tokyo best-track data.

~~**Scatter diagrams of relationship between predicted (y-axis) and best-track (x-axis) central pressures**~~

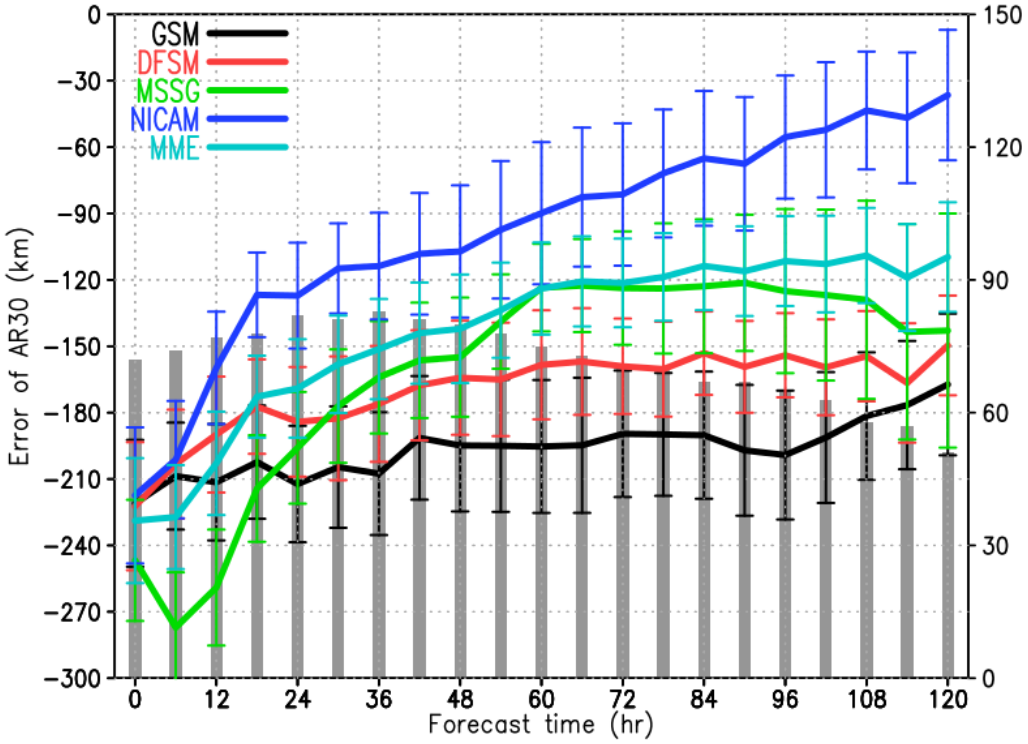

書式変更: 英語（英国），スペル チェックと文章校正を行う

書式変更: フォント：（日）ＭＳ 明朝

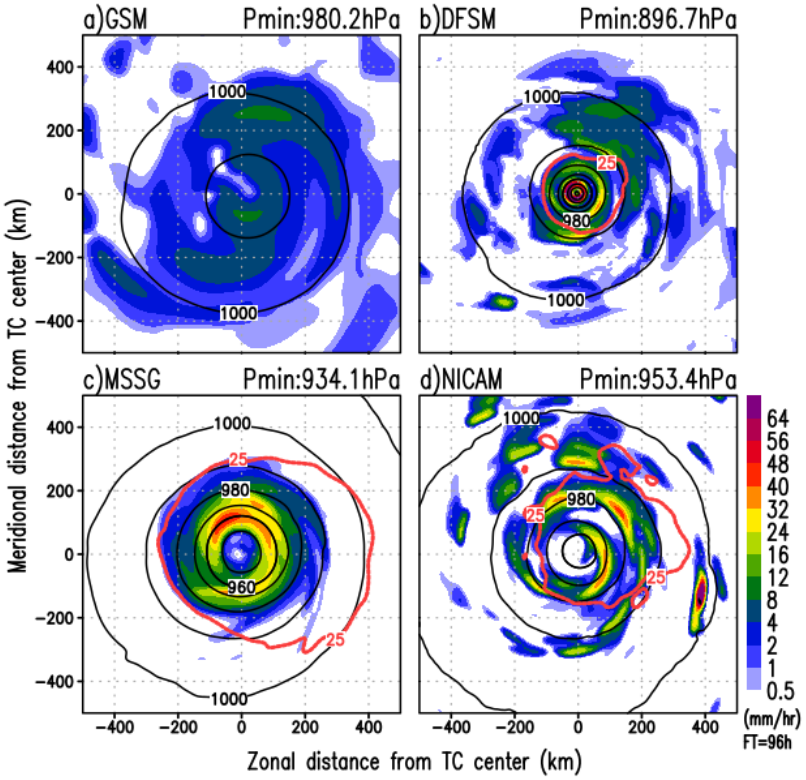

Figure 6. Errors in the averaged radius of the 30-knot wind (AR30) for GSM, DFSM, MSSG, NICAM and MME (in the second stage). Each grey bar indicates the number of samples at each forecast time (right-vertical axis). Error bars indicate 95% confidence levels of the AR30 difference between the prediction and the RSMC Tokyo best-track data.

~~**Horizontal distributions of precipitation (colour), sea level pressure (black contour) and wind speed 25 m s^{-1} (red contour) for Typhoon Wipha at FT = 96 h. Labels on horizontal and vertical axes shows zonal and meridional distances from TC centre (km), respectively. Contour intervals of sea level pressure are 10 hPa for > 960 hPa and 20 hPa for < 960 hPa. Plotted area is a 1000 km square and (x, y) = (0, 0) is set to TC centre.**~~

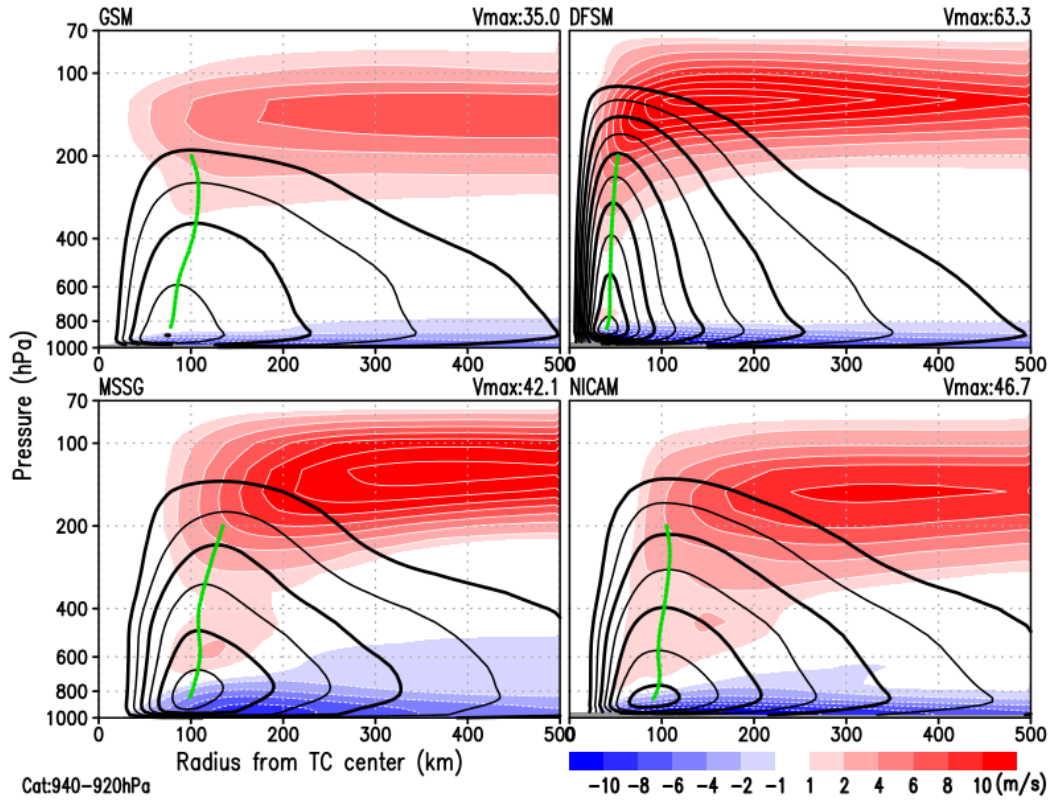

書式変更

Figure 7. Composite analysis of the radius–height cross section of the axisymmetric mean radial (shaded) and tangential (contour) wind speed for TCs at the time of the analysed central pressure between 920–940 hPa in the RSMC Tokyo best-track data. Contour intervals are 5 m s^{-1} (values > 15 m s^{-1} are plotted). ~~Green~~The green line depicts the RMW between 850 hPa and 200 hPa. ~~Grey~~The grey shading at the bottom of each panel is below the surface.

書式変更

書式変更

書式変更

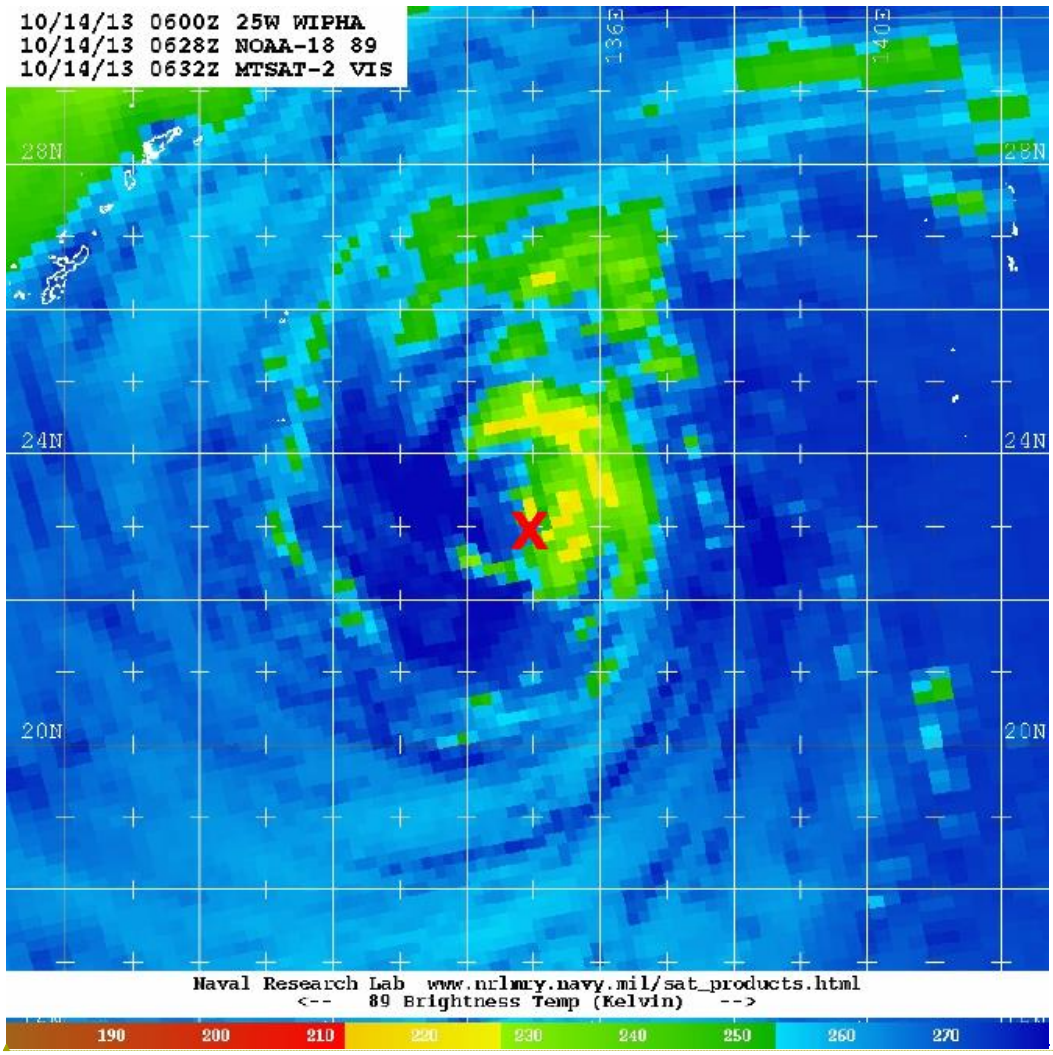

Figure 7 Brightness temperature observed by Advanced Microwave Sounding Unit – A (AMSU-A) channel 89 GHz onboard NOAA-18 at 14 October, 2013 06:28 UTC. (image courtesy of Naval Research Laboratory). Red "X" displays TC Wipha centre.

書式変更: フォント：（日）ＭＳ 明朝，フォントの色：赤

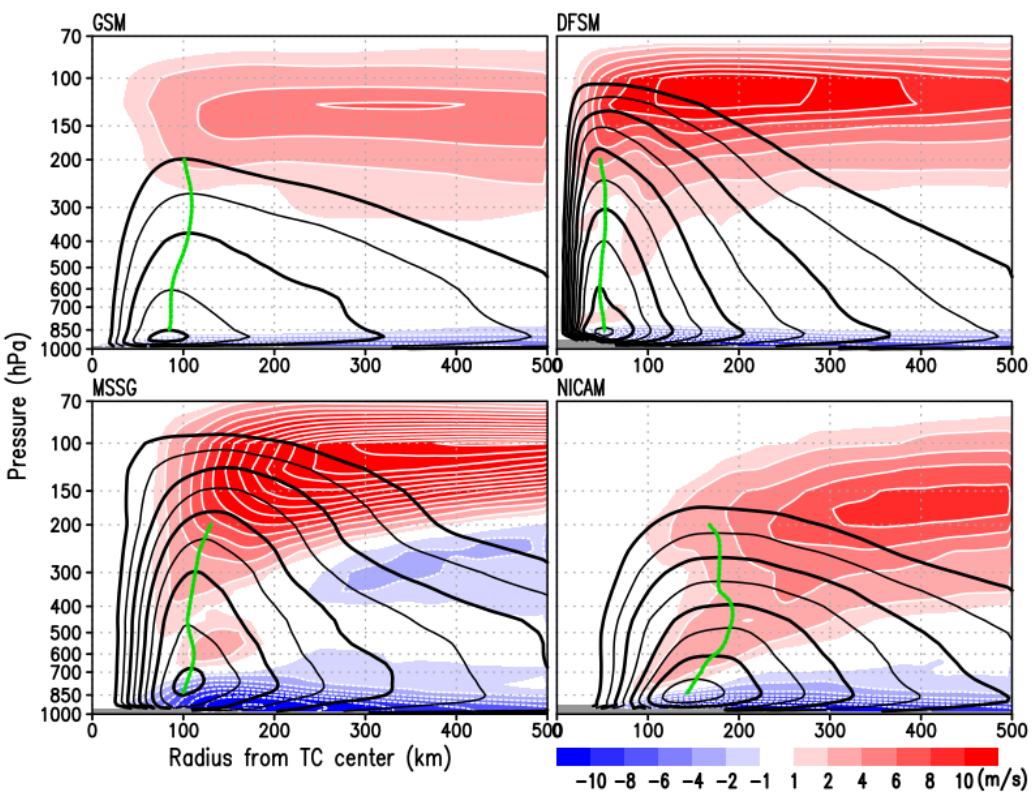

Figure 8 Composite analysis of r-z cross sections of axisymmetric mean radial (shaded) and tangential (contour) wind speeds. Contour intervals are 5 m s^{-1} (values > 15 m s^{-1} are plotted). Green line depicts RMW between 850 and 200 hPa. Grey shading at bottom of each panel is below the surface.

書式変更: フォント：（日）ＭＳ 明朝

書式変更: フォント：（日）ＭＳ 明朝

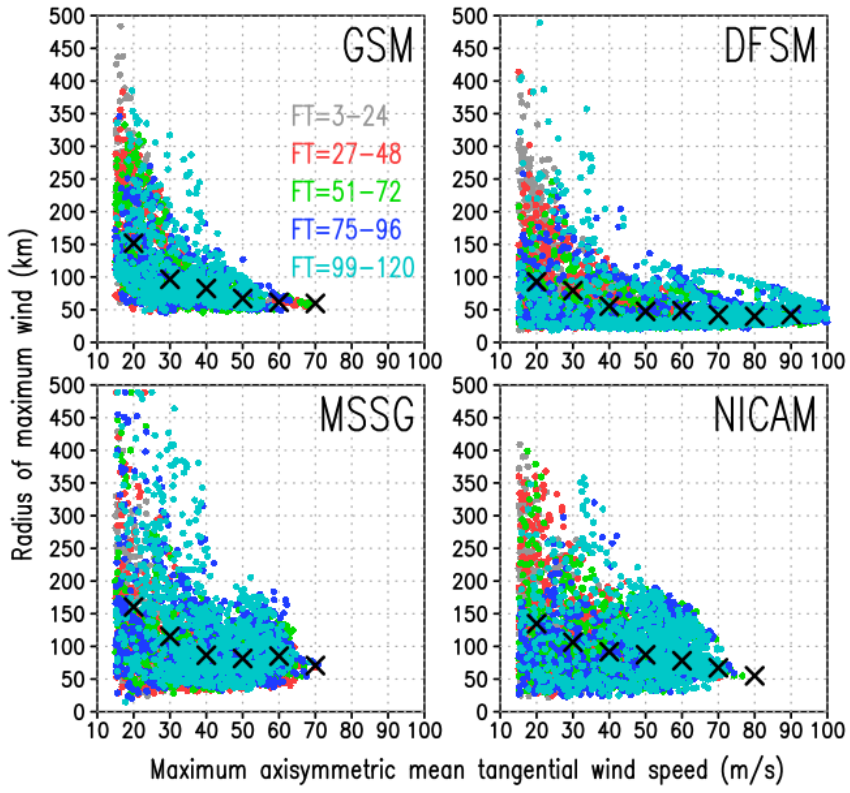

~~Figure 9 Scatter plot of maximum axisymmetric mean tangential wind speeds (x-axis; m s^{-1}) and radius of maximum wind speeds (RMW, in km). Colours show forecast times (in h) of 3–24 (grey), 27–48 (red), 51–72 (green), 78–96 (blue), and 99–120 (cyan). X marks indicate mean RMW for each intensity (e.g., "20" uses all cases in which intensity is between 15 and 25 m s^{-1})~~